FAST FOURIER TRANSFORMED ACOUSTIC RESONANCES WITH SONIC TRANSFORM

By

KENNETH C. MCGILL

A DISSERTATION PRESENTED TO THE GRADUATE SCHOOL
OF THE UNIVERSITY OF FLORIDA IN PARTIAL FULFILLMENT
OF THE REQUIREMENTS FOR THE DEGREE OF
DOCTOR OF PHILOSOPHY

UNIVERSITY OF FLORIDA

1990

Copyright 1990

by

Kenneth Charles McGill

DEDICATION

This work is dedicated to the three people whom I owe so much: To my mother Martha Senogles who gave me life; to my late wife Natalie McGill who gave me her life; and to my wife Susan McGill who is giving me a new life in my first child.

ACKNOWLEDGMENTS

I would like to thank Dr. S.O. Colgate personally for his support and guidance during the development of this technique.

I would also like to thank Chadin Dejsupa and Joe Shalosky for assisting in the construction of various parts of the apparatus, Casey Rentz for the use of his computer and Evan House for convincing me to join the Colgators.

In addition, I would like to thank Dr. Grant Schrag for the development of the tapered ram seal used for the electrical feed-throughs of the transducers, Dr. Cliff Watson for his assistance in programming the Fast Fourier Transform and Steve Miles for his contribution on the development of the magnetic pump.

Also, I thank my wife, Susan, for instructing me on the use of WordPerfect so that I could perfect the format of this dissertation.

TABLE OF CONTENTS

page

ACKNOWLEDGMENTS..... iv

LIST OF TABLES.....vii

LIST OF FIGURES..... ix

ABSTRACT..... xi

CHAPTERS

1 INTRODUCTION..... 1

2 THEORY..... 8

Theory of Design..... 9
Theory of Operation..... 18

3 EXPERIMENTAL..... 29

Interfacing..... 30
Apparatus..... 34
Spherical Cavity..... 34
Pump..... 35
The Bellows..... 37

4 DATA AND RESULTS..... 42

Time Domain Plots..... 44
Frequency Domain Plots..... 45
Sonic Domain Plots..... 46
Volume and Pressure Calibration..... 48

5 CONCLUSION..... 69

APPENDICES

A FAST FOURIER TRANSFORM SOURCE CODE..... 76

B SONIC TRANSFORM SOURCE CODE..... 80

C EQUATION OF STATE FOR ARGON SOURCE CODE..... 84

D DATA ACQUISITION SOURCE CODE..... 87

E DATA CONVERSION SOURCE CODE..... 93

BIBLIOGRAPHY..... 95

BIOGRAPHICAL SKETCH..... 97

LIST OF TABLES

page

Table 2-1. The values of the roots to the first derivative of a Bessel function of the first kind..... 12

Table 2-2. Reduced second virial coefficients for the Lennard-Jones 6-12 potential..... 20

Table 2-3. Reduced third virial coefficients and their derivatives for the Lennard-Jones 6-12 potential..... 22

Table 4-1. Low temperature time domain parameters of argon..... 53

Table 4-2. Low temperature frequency domain parameters of argon..... 54

Table 4-3. First sonic domain parameters of argon at low temperature..... 55

Table 4-4. Second sonic domain parameters of argon at low temperature..... 56

Table 4-5. Third sonic domain parameters of argon at low temperature..... 57

Table 4-6. Fourth sonic domain parameters of argon at low temperature..... 58

Table 4-7. High temperature time domain parameters of argon..... 59

Table 4-8. High temperature frequency domain parameters of argon..... 60

Table 4-9. First sonic domain parameters of argon at high temperature..... 61

Table 4-10. Second sonic domain parameters of argon at high temperature..... 62

Table 4-11. Third sonic domain parameters of argon at high temperature..... 63

Table 4-12. Fourth sonic domain parameters of argon at high temperature..... 64

Table 4-13. Outside volume calibration..... 65

Table 4-14. Total volume of apparatus..... 66

Table 4-15. Bellows volume calibration..... 67

Table 4-16. Compiled results of sonic speeds of argon at low and high temperatures for various roots..... 68

LIST OF FIGURES

page

Figure 3-1. Instrument rack..... 32

Figure 3-2. Spherical cavity sections and clamping flanges..... 36

Figure 3-3. Pump assembly..... 38

Figure 3-4. The bellows and bellows chamber..... 39

Figure 3-5. Apparatus assembly..... 41

Figure 4-1. Theoretical ADC signal for 350 m/s speed of sound..... 50

Figure 4-2. Theoretical ADC signal for 150 m/s and 350 m/s speeds of sound..... 50

Figure 4-3. FFT of theoretical ADC signal for 350 m/s speed of sound..... 51

Figure 4-4. FFT of theoretical ADC signal for 150 m/s and 350 m/s speeds of sound..... 51

Figure 4-5. ST of FFT of theoretical ADC signal for 350 m/s..... 52

Figure 4-6. ST of FFT of theoretical ADC signal for 150 m/s and 350 m/s speeds of sound..... 52

Figure 4-7. ADC signal of argon at low temperature..... 53

Figure 4-8. Expanded section of Figure 4-7..... 53

Figure 4-9. FFT of ADC signal of argon at low temperature..... 54

Figure 4-10. Expanded section of Figure 4-9..... 54

Figure 4-11. First ST of argon at low temperature..... 55

Figure 4-12. Expanded section of Figure 4-11..... 55

Figure 4-13. Second ST of argon at low temperature..... 56

Figure 4-14. Expanded section of Figure 4-13..... 56
Figure 4-15. Third ST of argon at low temperature..... 57
Figure 4-16. Expanded section of Figure 4-15..... 57
Figure 4-17. Fourth ST of argon at low temperature..... 58
Figure 4-18. Expanded section of Figure 4-17..... 58
Figure 4-19. ADC signal of argon at high temperature.... 59
Figure 4-20. Expanded section of Figure 4-19..... 59
Figure 4-21. FFT of ADC signal of argon at high temperature..... 60
Figure 4-22. Expanded section of Figure 4-21..... 60
Figure 4-23. First ST of argon at high temperature..... 61
Figure 4-24. Expanded section of Figure 4-23..... 61
Figure 4-25. Second ST of argon at high temperature..... 62
Figure 4-26. Expanded section of Figure 4-25..... 62
Figure 4-27. Third ST of argon at high temperature..... 63
Figure 4-28. Expanded section of Figure 4-27..... 63
Figure 4-29. Fourth ST of argon at high temperature..... 64
Figure 4-30. Expanded section of Figure 4-29..... 64
Figure 4-31. Outside volume calibration..... 65
Figure 4-32. Total volume of apparatus..... 66
Figure 4-33. Bellows calibration plot..... 67

Abstract of Dissertation Presented to the Graduate School of the University of Florida in Partial Fulfillment of the Requirements for the Degree of Doctor of Philosophy

FAST FOURIER TRANSFORMED ACOUSTIC RESONANCES WITH SONIC TRANSFORM

By

Kenneth C. McGill

December 1990

Chairman: S.O. Colgate
Major Department: Chemistry

In this study, a novel approach for detecting one or more speeds of sound was developed. By employing a Sonic Transform (ST), the data are transformed in real time to a domain that is directly related to the speed of sound within a cavity. The transform is of order $< n^2$ and is equivalent to a Fast Fourier Transform in computation time. The study contains a discussion of the apparatus design as well as interfacing techniques involved in its operation. Source code and algorithms that describe the analysis and data acquisition in detail are also contained within the study.

CHAPTER 1
INTRODUCTION

The measurement of state variables is of interest to researchers in thermodynamics. The two most commonly measured state variables are temperature and pressure. Techniques for their measurement have been developed that have high accuracy and speed of operation and are relatively easy to use. The equation of state for even the simplest system, for example, a single component gas, requires at least another variable. For whatever additional variable is chosen, it is desirable that its measurement be performed as quickly and as easily as those of temperature and pressure.

The most commonly measured third state variable is volume. The measurement of volume is often done by a batch process where a fluid substance is placed in a vessel of calibrated volume. This process is time-comsuming and is prone to error. Individual error can occur in recording the measurement and it is impossible to do real time processing of the data.

There are other state variables that could be measured, such as entropy, enthalpy, and free energy, but these are even more difficult to measure in a batch process or in real time. If a reliable equation of state relating three state variables is available, then the magnitude of the third

variable may be calculated after measuring the other two. This method works well for single component gases, but it is not very accurate for multicomponent mixtures of gases or for any gas near its critical region.

In this work, emphasis is placed on the development of a novel sonic speed measurement technique to facilitate the use of this state variable along with temperature, pressure and volume in physical relationships. An effort to make the measurement of the speed of sound as accurate and as easy as temperature and pressure has been made; that is, a process has been developed that can operate in real time with high accuracy and with little interaction from the user. The measurements of volume and speed of sound are similar; one way to measure the volume of a gas involves the geometry of the vessel in which the gas is contained and, similarly, one way to measure the speed of sound in a gas involves the geometry of the vessel in which the gas is contained. By knowing the geometry of the vessel, the volume can be calculated by measuring the dimensions of the vessel. The speed of sound can be found by measuring the acoustic resonances within the cavity. The speed of sound is also dependent on the density and mass of the gas being measured.

An accurate method for measuring the speed of sound involves examination of the resonances that occur in an acoustic cavity. The selection of the geometry of the cavity can make a significant difference in the ease of

interpretation of the resonance frequencies. For example, resonances in a cylindrical cavity are complicated by problems, such as unresolved modes and viscous drag along the longitudinal walls. These problems have been examined in detail elsewhere.[1]

Another potential problem with any shaped cavity results from a precondensation effect that occurs on the surface of the cavity.[2] This effect appears most strongly at low frequencies in resonators with large surface-to-volume ratios. To avoid these problems, a spherical cavity was chosen since: 1) Viscous drag does not occur for the radial vibrations within a spherical cavity; 2) surface-to-volume ratio is minimized for spherical geometry; and 3) the acoustic energy is highest at the center of the sphere.

In a study that included a treatment of the precondensation effect in a spherical cavity, the speed of sound of a gas was measured with an accuracy approaching ± 0.0005% or 5 ppm.[3] Neglecting the precondensation effect,

---

[1] J.B. Mehl and M.R. Moldover, "Precision Acoustic Measurements with a Spherical Resonator: Ar and C_2H_4," Journal of Chemical Physics 74 (April 1981): 4062-4077; A.R. Colclough, "Systematic Errors in Primary Acoustic Thermometry in the Range 2-20 K," Metrologia 9 (1973): 75.

[2] J.B. Mehl and M.R. Moldover, "Precondensation Phenomena in Acoustic Measurements," Journal of Chemical Physics 77 (July 1982): 455-465.

[3] M.R. Moldover, J.B. Mehl, and M. Greenspan, "Gas-Filled Spherical Resonators: Theory and Experiment," Journal of the Acoustical Society of America 79 (February 1986): 253-271.

accuracies of 0.01% are readily obtained for physical properties inferred from sonic speed measurements, these include reference state heat capacities,[4] thermophysical properties of alkanes,[5] and heat capacity ratios.[6] In all of these experiments, the first step is to analyze a frequency spectrum and then select only a few of the resonances, at most five or six depending upon the experiment, to measure the speed of sound.[7] This interaction from the user requires an intuition as to where the resonances occur, and locating them with confidence is often tedious and can take a considerable amount of experimental time. This places an added burden on the maintenance of the system's state. The measurement of temperature and pressure can be very accurate, but maintaining them for long periods of time is not easy. All

---

[4] S.O. Colgate, C.F. Sona, K.R. Reed, and A. Sivaraman, "Experimental Ideal Gas Reference State Heat Capacities of Gases and Vapors," Journal of Chemical and Engineering Data 35 (1990): 1-5.

[5] M.B. Ewing, A.R.H. Goodwin, and J.P.M. Trusler, "Thermophysical Properties of Alkanes from Speeds of Sound Determined Using a Spherical Resonator 3. n-Pentane," Journal of Chemical Thermodynamics 21 (1989): 867-877.

[6] S.O. Colgate, K.R. Williams, K. Reed, and C. Hart, "C_p/C_v Ratios by the Sound Velocity Method Using a Spherical Resonator," Journal of Chemical Education 64 (June 1987): 553-556.

[7] M.B. Ewing, M.L. McGlashan, and J.P.M. Trusler, "The Temperature-Jump Effect and the Theory of the Thermal Boundary Layer for a Spherical Resonator, Speeds of Sound in Argon at 273.16 K," Metrologia 22 (1986): 93-102.

of these methods assume that only one speed of sound is present within the medium of interest. If multiple speeds of sound are present within a medium, the difficulties of the job of analysis are seriously compounded. Ideally, a method that can identify the resonances as well as calculate a close approximation of the speed of sound very quickly would represent a significant advance in the art of sonic speed measurements.

Since the number of possible resonances is of the order of the number of molecules, it is for all practical purposes infinite. Ideally, a broad band of resonances should be used to determine the speed of sound within the gas. One such attempt at measuring a truncated set of resonances was made by Tewfik et al.[8] This study modeled two dimensional waves such as the waves on the ocean. Their method involved a rather large calculation employing Householder routines to solve an nXn linear matrix problem. A Householder routine[9] is an operation of order n^3 for which even a relatively small set of resonances becomes costly in computation time. Hence, although the Householder routine is capable of high accuracy, it can not be considered useful as a real time process.

---

[8] A.H. Tewfik, B.C. Levy, and A.S. Willsky, "An Eigenstructure Approach for the Retrieval of Cylindrical Harmonics," Signal Processing 13 (September 1987): 121-139.

[9] G.H. Golub and C.F. Van Loan, Matrix Computations (Baltimore: Johns Hopkins University Press, 1985), 38.

In order to overcome these boundaries, a technique was developed in the present work to transform the Fourier coefficients of a captured time domain signal to the sonic domain. Once in this domain, the speed of sound is easily determined. For the development of this technique, a spherical cavity and a truncated set of resonances were used. The truncated set of resonances was transformed from a measured time domain signal to the sonic domain using a transform operation of order $n\log_2 n + nm$, where m is the number of resonances.

To test the method, a theoretical (computer synthesized) frequency spectrum was created and then the speed (or speeds) of sound were found from the spectrum and compared to the speed (or speeds) of sound used to produce the spectrum. Once satisfied that the method could reproduce the speed of sound from a simulated spectrum, some experimental spectra were analyzed. The transformed speeds of sound obtained from these experimental spectra were then compared to known values, which for the gas in question, argon, have been shown to be in accord with those directly calculated using a truncated virial equation of state. The transformed speeds of sound may be lower than the calculated speeds since the latter are the speeds of sound at zero frequency and the transformed ones are an average speed of sound over all the frequencies within the spectrum.

The following chapters describe the theory of design as well as the theory of operation of this transformation technique. The design of the apparatus is similar to other acoustic devices with a few exceptions. The seal technology employed allows operation over wider temperature and pressure ranges. Another unique feature of the apparatus is the ability to vary its volume with a specially designed bellows assembly. This apparatus has the capability to measure four state variables simultaneously. In addition, the source code for all measurement techniques has been included in the appendices to describe the operation of the apparatus in detail.

CHAPTER 2
THEORY

Two basic theoretical constructs central to the present novel sonic speed technique are explained in this chapter--the theory of design and the theory of operation. The theory of design begins with established theories of wave phenomena and applies modern computational methodologies to them. A new algorithm developed here facilitates the computations.

The theory of operation is presented to reveal the order of events that lead to the measurement of the speed of sound with this technique. The equations and operational bounds may seem trivial to anyone familiar with Fast Fourier Transform (FFT) techniques, but, to the newcomer, these will likely seem arbitrary and unbounded. They are, in fact, very closely interrelated. The two parameters that govern the operation of any FFT spectrometer are the buffer size and the sample rate of the ADC; other parameters may be deduced from them. The operation of many of the basic theories described are transparent to the user since they are contained mainly within the source code given in the appendices.

Theory of Design

The dynamics associated with the acoustical field of a nondissipating gas were first examined by Rayleigh in 1872.[1] Rayleigh's development revealed a basis set of resonant frequencies of sound for a gas in a cavity. Experimentally these frequencies have heretofore been measured by observing the response of the gas to a slowly varying periodic stimulus. The present work is concerned with obtaining the information implicit in the frequency spectrum very rapidly. Acquisition of the frequency domain may be accomplished by a Fast Fourier Transform (FFT) of a time domain signal from an Analog to Digital Converter (ADC). Through a Sonic Transformation (ST) of the Fourier coefficients, this information can be further transformed into the sonic domain which readily reveals the speed of sound and other features of the acoustic field.

First, assume there exists a velocity potential ψ such that

$$\vec{v} = -\nabla\psi \qquad \text{Equation 2-1.}$$

where v is the velocity of the gas. The standing wave produced in the gas with a speed of sound (c) is related to ψ by the standard wave equation

---

[1] J.W.S. Rayleigh, Theory of Sound (New York: Dover, 1894), reprinted 1945, Section 331.

$$\nabla^2\psi = \frac{1}{c^2}\frac{\partial^2\psi}{\partial t^2}. \qquad \text{Equation 2-2.}$$

Assuming a time separable solution to the above equation

$$\psi = \psi_0(r,\theta,\varphi)\,e^{i\omega t}, \qquad \text{Equation 2-3.}$$

where ψ_0 is then the solution to a scaler Helmholtz equation

$$\nabla^2\psi_0 + \left(\frac{\omega}{c}\right)^2\psi_0 = 0, \qquad \text{Equation 2-4.}$$

then the analytical expression for ψ_0 [2] is

$$\psi_0 = j_l\left(\frac{\omega}{c}r\right) P_l^m(\cos(\theta))\,(A\sin(m\varphi) + B\cos(m\varphi)).$$

Equation 2-5.

The function j_l is a Bessel function of the first kind and P_l^m is an associated Legendre polynomial in $\cos(\theta)$. Since, by definition, a nondissipating gas is contained, the boundary condition of the radial component is that the velocity of the gas is zero at the rigid wall

$$\int_{Surf}^{b} \vec{v}\cdot d\vec{a} = 0. \qquad \text{Equation 2-6.}$$

---

[2] H.G. Ferris, "The Free Vibrations of a Gas Contained within a Spherical Vessel," Journal of the Acoustical Society of America 24 (January 1952): 57.

For a spherical cavity, the surface is described by

$$d\vec{a} = g^2 \sin(\theta)\, d\theta d\varphi \hat{r}, \qquad \text{Equation 2-7.}$$

where g is a geometric factor or the radius of the spherical cavity. Substitution of the gradient of ψ in Equation 2-6 yields

$$-\int_{Surf}^{b}_{a} P_l^m(\cos(\theta))\,(A\sin(m\varphi)+B\cos(m\varphi))\, g^2 \sin(\theta)\, d\theta d\varphi \frac{\partial j_l}{\partial r}\Big|_{r=g} = 0.$$

Equation 2-8.

Since this must be zero for all values of a and b, then

$$\frac{\partial}{\partial r} j_l\left(\frac{\omega}{c} r\right)\Big|_{r=g} = 0. \qquad \text{Equation 2-9.}$$

For a given value of l, there are an infinite number of roots for the above relation. The lowest positive root is denoted by n=1, the next root is n=2, the following n=3, and so forth. These integral values represent the modes of vibration for that given l. The roots of the above relations have been calculated in increasing magnitude as shown in Table 2-1.[3]

---

[3] Ferris.

Table 2-1. The values of the roots to the first derivative of a Bessel function of the first kind.

i	R_i	l	n
1	2.08158	1	1
2	3.34209	2	1
3	4.49341	0	1
4	4.51408	3	1
5	5.64670	4	1
6	5.94036	1	2
7	6.75643	5	1
8	7.28990	2	2
9	7.72523	0	2
10	7.85107	6	1
11	8.58367	3	2
12	8.93489	7	1
13	9.20586	1	3
14	9.84043	4	2
15	10.0102	8	1
16	10.6140	2	3
17	10.9042	0	3
18	11.0703	5	2
19	11.0791	9	1
20	11.9729	3	3
21	12.1428	10	1
22	12.2794	6	2
23	12.4046	1	4
24	13.2024	11	1
25	13.2956	4	3
26	13.4721	7	2
27	13.8463	2	4
28	14.0663	0	4
29	14.2580	12	1
30	14.5906	5	3
31	14.6513	8	2
32	15.2446	3	4
33	15.3108	13	1
34	15.5793	1	5
35	15.8193	9	2
36	15.8633	6	3
37	16.3604	14	1
38	16.6094	4	4
39	16.9776	10	2
40	17.0431	2	5
41	17.1176	7	3
42	17.2207	0	5

Table 2-1 continued.

i	R_i	l	n
43	17.4079	15	1
44	17.9473	5	4
45	18.1276	11	2
46	18.3565	8	3
47	18.4527	16	1
48	18.4682	3	5
49	18.7428	1	6
50	19.2628	6	4
51	19.2704	12	2
52	19.4964	17	1
53	19.5819	9	3
54	19.8625	4	5
55	20.2219	2	6
56	20.3714	0	6
57	20.4065	13	2
58	20.5379	18	1
59	20.5596	7	4
60	20.7960	10	3
61	21.2312	5	5
62	21.5372	14	2
63	21.5779	19	1
64	21.6667	3	6
65	21.8401	8	4
66	21.8997	1	7
67	22.0000	11	3
68	22.5781	6	5
69	22.6165	20	1
70	22.6625	15	2
71	23.0829	4	6
72	23.1067	9	4
73	23.1950	12	3
74	23.3906	2	7
75	23.5194	0	7
76	23.6534	21	1
77	23.7832	16	2
78	23.9069	7	5
79	24.3608	10	4
80	24.3821	13	3
81	24.4749	5	6
82	24.6899	22	1
83	24.8503	3	7
84	24.8995	17	2

A solution to the above equation occurs when

$$\frac{\omega_i}{c} g = R_i \qquad \text{Equation 2-10.}$$

and the frequency of the standing wave within the cavity at speed c is then

$$\omega_i = 2\pi f_i = \frac{R_i\, c}{g}, \qquad \text{Equation 2-11.}$$

where g is a geometric factor and R_i is the ith tabulated root.

The previous equation describes the frequency basis for all standing waves or resonant excitations in the cavity. Experimentally, the resonant frequencies are acquired in the Fourier format (see Appendix A) where

$$F^F(t) = \sum_{p}^{\infty} (A_p \sin(\omega_p t) + B_p \cos(\omega_p t)). \qquad \text{Equation 2-12.}$$

If multiple speeds of sound occur within the cavity medium, each having an almost infinite number of resonant frequencies, the job of determining the speeds of sound from the corresponding frequencies is tedious. Even with a truncated basis of roots (as in Table 2-1), finding the speed is not easy and requires considerable analysis. The

ST developed below facilitates this task. It transforms the coefficients of the FFT directly to the sonic speed domain.

Consider a system through which sound propagates at one or more speeds. Let the associated frequencies be weighted by some values k_i, where

$$F^S(t) = \sum_{i}^{\infty} k_i f(c_i, t) \qquad \text{Equation 2-13.}$$

and

$$f(c_i, t) = \sum_{j}^{\infty} (a_{ij}\sin(gc_iR_jt) + b_{ij}\cos(gc_iR_jt)) . \qquad \text{Equation 2-14.}$$

If we assume that all signals detected in the Fourier coefficients are acoustic resonances

$$F^F(t) = F^S(t), \qquad \text{Equation 2-15.}$$

then it follows that

$$A_p = \sum_{i}^{\infty}\sum_{j}^{\infty} k_i a_{ij} \delta(\omega_p, gc_iR_j) \qquad \text{Equation 2-16.}$$

where the value of δ is as follows,

$$\delta(\omega_p, gc_iR_j) = \delta_{pij} = \begin{cases} 1, \omega_p = gc_iR_j \\ 0, \omega_p \neq gc_iR_j \end{cases}. \quad \text{Equation 2-17.}$$

The values of k_i are of greater interest than the Fourier coefficients. One method to acquire n coefficients for a truncated sum of m roots would be to perform n truncated least square operations of order 2m+1 to obtain n functions $f(c_i,t)$ and then perform one more least square operation of order n to obtain the coefficients k_i. Each least square operation is approximately an n-cubed operation (FLOPs[4] $\propto n^3$). By performing the transformation shown below, weights that are proportional to k_i can be obtained with considerably fewer FLOPs.

Let

$$w_l = \frac{1}{n}\sum_{m}^{n}\sum_{p}^{\infty} A_p\delta_{plm}, \quad \text{Equation 2-18.}$$

then by substituting A_p from Equation 2-16 into the above expression,

---

[4] FLOP is a FLoating point OPeration (see Chapter 3, Theory of Operation).

$$w_l = \frac{1}{n}\sum_{m}^{n}\sum_{p}^{\infty}\sum_{i}^{\infty}\sum_{j}^{\infty} k_l a_{ij}\delta_{pij}\delta_{plm}. \quad \text{Equation 2-19.}$$

Since l is fixed, then for a given m and p, the only nonzero values occurs when i=l and j=m. This reduces the above expression to

$$w_l = \frac{1}{n}\sum_{m}^{n}\sum_{p}^{\infty} k_l a_{lm}\delta_{plm}. \quad \text{Equation 2-20.}$$

For a given l and m, there is only one nonzero value p, hence

$$w_l = \frac{1}{n}\sum_{m}^{n} k_l a_{lm} = k_l \frac{1}{n}\sum_{m}^{n} a_{lm} = k_l \overline{a_l} \quad \text{Equation 2-22.}$$

where $\overline{a}_l$ is the average amplitude over n roots of the lth speed. Most importantly, this result shows that this choice of weights is directly proportional to the sonic coefficients k_l. The relative values of w_l cannot be used for determining relative values of k_l. Since there is an overlap of different R_i values, the weights can be used to detect the presence of resonant speed of sound within the cavity.

Theory of Operation

For the purpose of evaluating the sonic transform technique, its use on a gas with known properties is required. Argon was chosen for this purpose because of its relative simplicity and well-documented physical behavior. The speed of sound in argon has been carefully measured and shown to be in agreement with values calculated with the virial equation of state.[5]

At moderate pressures (< 10 atm) two terms in the virial expansion are sufficient to give sonic speeds within experimental uncertainty. For this work the sonic speed in argon was calculated from the virial equation of state (truncated after the third term) using reduced virial coefficients obtained from a Lennard-Jones 6-12 potential. The speed of sound at zero frequency[6] may be related to either the adiabatic or isothermal partial derivative of pressure with respect to molar density. Specifically, the square of the speed of sound is

$$c_0^2 = \frac{1}{M}\left(\frac{\partial P}{\partial \rho}\right)_S = \frac{\gamma}{M}\left(\frac{\partial P}{\partial \rho}\right)_T, \qquad \text{Equation 2-22.}$$

---

[5] R. Byron Bird, "Numerical Evaluation of the Second Virial Coefficient," The Virial Equation of State CM-599 (Madison: University of Wisconsin, May 10, 1950), 47-52.

[6] J.O. Hirschfelder, C.F. Curtiss, and R.B. Bird, Molecular Theory of Gases and Liquids (New York: Wiley and Sons, 1954), 369.

where P is pressure, M is the molecular weight and ρ is the molar density. Using the constant temperature form of the above equation, where γ is the ratio of heat capacities, the speed of sound can be found by solving for the individual values of C_p, C_v and the constant temperature derivative. There is no equation of state that can be expressed in a single analytical expression that has high enough accuracy for this experiment. The best possible solution is a truncated virial equation with numerically calculated coefficients at various temperatures. The values of the second virial coefficients are given in Table 2-2 and the values of the third virial coefficients are given in Table 2-3. The accuracy of this numerical solution has been investigated by Bird.[7] Using the truncated virial equation of state in terms of reduced virial coefficients given by:

Key Terms, Symbols and Definitions for Truncated Virial Equation of State

B = Second Virial Coefficient	k = Boltzmann's constant
C = Third Virial Coefficient	R = Gas constant
$b_0 = \frac{2}{3}\pi\tilde{N}\sigma^3$	$B^* = B/b_0$
σ = Lennard-Jones 6-12 collision diameter	$C^* = C/b^2_0$
ϵ = Lennard-Jones 6-12 maximum energy attraction or depth of potential well	$T^* = kT/\epsilon$
	$\tilde{N}$ = Avogadro's Number

[7] Bird.

Table 2-2. Reduced second virial coefficients for the Lennard-Jones 6-12 potential.

T*	B*	B_1*	B_2*	B_1*-B*
0.30	-27.880581	76.607256	-356.87679	104.488
0.35	-18.754895	45.247713	-189.46536	64.003
0.40	-13.798835	30.267080	-116.36604	44.066
0.45	-10.754975	21.989482	-78.87795	32.744
0.50	-8.720205	16.923690	-57.33952	25.644
0.55	-7.2740858	13.582156	-43.88245	20.8563
0.60	-6.1979708	11.248849	-34.91869	17.4468
0.65	-5.3681918	9.5455096	-28.64050	14.9137
0.70	-4.7100370	8.2571145	-24.06266	12.9672
0.75	-4.1759283	7.2540135	-20.61311	11.4299
0.80	-3.7342254	6.4541400	-17.94190	10.1884
0.85	-3.3631193	5.8034061	-15.82546	9.1665
0.90	-3.0471143	5.2649184	-14.11557	8.3120
0.95	-2.7749102	4.8127607	-12.71081	7.5877
1.00	-2.5380814	4.4282616	-11.53985	6.9663
1.05	-2.3302208	4.0976659	-10.55133	6.4279
1.10	-2.1463742	3.8106421	-9.70744	5.9570
1.15	-1.9826492	3.5592925	-8.97985	5.5419
1.20	-1.8359492	3.3374893	-8.34700	5.1734
1.25	-1.7037784	3.1404074	-7.79217	4.8442
1.30	-1.5841047	2.9642040	-7.30227	4.5483
1.35	-1.4752571	2.8057826	-6.86692	4.2810
1.40	-1.3758479	2.6626207	-6.47777	4.0385
1.45	-1.2847160	2.5326459	-6.12805	3.8174
1.50	-1.2008832	2.4141403	-5.81225	3.6150
1.55	-1.1235183	2.3056683	-5.52578	3.4292
1.60	-1.0519115	2.2060215	-5.26485	3.2579
1.65	-0.98545337	2.1141772	-5.02628	3.0996
1.70	-0.92361639	2.0292621	-4.80738	2.9529
1.75	-0.86594279	1.9505276	-4.60587	2.8165
1.80	-0.81203328	1.8773287	-4.41980	2.6894
1.85	-0.76153734	1.8091057	-4.24750	2.5706
1.90	-0.71414733	1.7453722	-4.08753	2.4595
1.95	-0.66959030	1.6857016	-3.93863	2.3553
2.00	-0.62762535	1.6297207	-3.79972	2.2573
2.10	-0.55063308	1.5275444	-3.54814	2.0782
2.20	-0.48170997	1.4366294	-3.32647	1.9183
2.30	-0.41967761	1.3552188	-3.12974	1.7749
2.40	-0.36357566	1.2819016	-2.95401	1.6455
2.50	-0.31261340	1.2155320	-2.79614	1.5281
2.60	-0.26613345	1.1551691	-2.65355	1.4213
2.70	-0.22358626	1.1000353	-2.52416	1.3236
2.80	-0.18450728	1.0494802	-2.40623	1.2340

Table 2-2 continued.

T*	B*	B_1*	B_2*	B_1*-B*
2.90	-0.14850215	1.0029572	-2.29831	1.1515
3.00	-0.11523390	0.9600031	-2.19920	1.0752
3.10	-0.08441245	0.9202229	-2.10785	1.0046
3.20	-0.05578696	0.8832774	-2.02340	0.93906
3.30	-0.02913997	0.8488746	-1.94511	0.87802
3.40	-0.00428086	0.8167606	-1.87231	0.82104
3.50	0.01895684	0.7867145	-1.80447	0.76776
3.60	0.04072012	0.7585430	-1.74108	0.71782
3.70	0.06113882	0.7300758	-1.68174	0.67094
3.80	0.08032793	0.7071630	-1.62605	0.62684
3.90	0.09839014	0.6836715	-1.57371	0.58528
4.00	0.11541691	0.6614830	-1.52441	0.54607
4.10	0.13149021	0.6404922	-1.47789	0.50900
4.20	0.14668372	0.6206045	-1.43394	0.47392
4.30	0.16106381	0.6017352	-1.39234	0.44067
4.40	0.17469039	0.5838082	-1.35291	0.40912
4.50	0.18761774	0.5667545	-1.31548	0.37914
4.60	0.19989511	0.5505118	-1.27991	0.35062
4.70	0.21156728	0.5350237	-1.24606	0.32346
4.80	0.22267507	0.5202387	-1.21381	0.29756
4.90	0.23325577	0.5061101	-1.18305	0.27285
5.00	0.24334351	0.4925951	-1.15367	0.24925
6.00	0.32290437	0.3839722	-0.919393	0.06107
7.00	0.37608846	0.3082566	-0.757930	-0.06783
8.00	0.41343396	0.2524801	-0.639879	-0.16095
9.00	0.44059784	0.2097011	-0.549792	-0.23090
10.00	0.46087529	0.1758670	-0.478779	-0.28501
20.00	0.52537420	0.0286638	-0.170403	-0.49671
30.00	0.52692546	-0.0174929	-0.072012	-0.54442
40.00	0.51857502	-0.0393115	-0.024109	-0.55789
50.00	0.50836143	-0.0516478	0.003927	-0.56001
60.00	0.49821261	-0.0593621	0.022147	-0.55758
70.00	0.48865069	-0.0645039	0.034817	-0.55316
80.00	0.47979009	-0.0680819	0.044056	-0.54787
90.00	0.47161504	-0.0706470	0.051031	-0.54226
100.00	0.46406948	-0.0725244	0.056441	-0.53659
200.00	0.41143168	-0.0775400	0.077296	-0.48897
300.00	0.38012787	-0.0765245	0.081397	-0.45665
400.00	0.35835117	-0.0747534	0.082055	-0.43310

Source: J.O. Hirschfelder, C.F. Curtiss, and R.B. Bird, Molecular Theory of Gases and Liquids (New York: Wiley and Sons, 1954), 1114.

Table 2-3. Reduced third virial coefficients and their derivatives for the Lennard-Jones 6-12 potential.

T*	C*	C_1*	C_2*
0.70	-3.37664	28.68	-220.
0.75	-1.79197	18.05	-140.
0.80	-0.84953	11.60	-92.1
0.85	-0.27657	7.561	-62.1
0.90	0.07650	4.953	-42.7
0.95	0.29509	3.234	-29.8
1.00	0.42966	2.078	-21.0
1.05	0.51080	1.292	-14.9
1.10	0.55762	0.7507	-10.6
1.15	0.58223	0.3760	-7.52
1.20	0.59240	0.1159	-5.29
1.25	0.59326	-0.0646	-3.66
1.30	0.58815	-0.1889	-2.46
1.35	0.57933	-0.2731	-1.57
1.40	0.56831	-0.3288	-0.910
1.45	0.55611	-0.3641	-0.420
1.50	0.54339	-0.3845	-0.050
1.55	0.53059	-0.3943	0.224
1.60	0.51803	-0.3963	0.427
1.65	0.50587	-0.3929	0.572
1.70	0.49425	-0.3858	0.680
1.75	0.48320	-0.3759	0.755
1.80	0.47277	-0.3643	0.806
1.85	0.46296	-0.3516	0.837
1.90	0.45376	-0.3382	0.854
1.95	0.44515	-0.3245	0.859
2.00	0.43710	-0.3109	0.856
2.10	0.42260	-0.2840	0.830
2.20	0.40999	-0.2588	0.794
2.30	0.39900	-0.2355	0.749
2.40	0.38943	-0.2142	0.700
2.50	0.38108	-0.1950	0.651
2.60	0.37378	-0.1777	0.602
2.70	0.36737	-0.1621	0.557
2.80	0.36173	-0.1482	0.514
2.90	0.35675	-0.1358	0.473
3.00	0.35234	-0.1247	0.439

Table 2-3 continued.

T*	C*	C_1*	C_2*
3.10	0.34842	-0.1148	0.400
3.20	0.34491	-0.1060	0.369
3.30	0.34177	-0.09826	0.340
3.40	0.33894	-0.09133	0.313
3.50	0.33638	-0.08510	0.288
3.60	0.33407	-0.07963	0.266
3.70	0.33196	-0.07462	0.246
3.80	0.33002	-0.07024	0.227
3.90	0.32825	-0.06634	0.210
4.00	0.32662	-0.06286	0.194
4.10	0.32510	-0.05989	0.183
4.20	0.32369	-0.05709	0.169
4.30	0.32238	-0.05458	0.156
4.40	0.32115	-0.05237	0.145
4.50	0.32000	-0.05040	0.134
4.60	0.31891	-0.04865	0.125
4.70	0.31788	-0.04712	0.116
4.80	0.31690	-0.04579	0.108
4.90	0.31596	-0.04461	0.100
5.00	0.31508	-0.04359	0.0934
6.00	0.30771	-0.03893	0.0449
7.00	0.30166	-0.03989	0.0258
8.00	0.29618	-0.04231	0.0192
9.00	0.29103	-0.04529	0.0183
10.00	0.28610	-0.04825	0.0199
20.00	0.24643	-0.06437	0.0502
30.00	0.21954	-0.06753	0.0654
40.00	0.20012	-0.06714	0.0717
50.00	0.18529	-0.06566	0.0742
60.00	0.17347	-0.06388	0.0750
70.00	0.16376	-0.06203	0.0748
80.00	0.15560	-0.06025	0.0741
90.00	0.14860	-0.05857	0.0732
100.00	0.14251	-0.05700	0.0722
200.00	0.10679	-0.04599	0.0619
300.00	0.08943	-0.03970	0.0547
400.00	0.07862	-0.03551	0.0496

Source: J.O. Hirschfelder, C.F. Curtiss, and R.B. Bird, Molecular Theory of Gases and Liquids (New York: Wiley and Sons, 1954), 1116.

$$B_1^* = T^* \left(\frac{dB^*}{dT^*} \right) \qquad C_1^* = T^* \left(\frac{dC^*}{dT^*} \right)$$
$$B_2^* = T^{*2} \left(\frac{d^2 B^*}{dT^{*2}} \right) \qquad C_2^* = T^{*2} \left(\frac{d^2 C^*}{dT^{*2}} \right) . \qquad \text{Equation 2-23.}$$

The constant pressure and constant volume heat capacities, respectively, are given by

$$C_P = R \left(\frac{5}{2} - \frac{B^{*2}}{V^*} + \left(\frac{(B^* - B_1^*)^2 - C^* + C_1^* - \frac{1}{2} C_2^*}{(V^*)^2} \right) \right) \qquad \text{Equation 2-24.}$$

and

$$C_V = \left(\frac{3}{2} - \frac{2B_1^* + B_2^*}{V^*} - \frac{2C_1^* + C_2^*}{2(V^*)^2} \right) . \qquad \text{Equation 2-25.}$$

The constant temperature derivative is given by

$$P = \frac{RT}{V} \left(1 + \frac{B^*}{V^*} + \frac{C^*}{(V^*)^2} \right)$$
$$\left(\frac{\partial P}{\partial \frac{1}{V}} \right)_T = -RT \left(1 + 2\frac{B^*}{V^*} + 3\frac{C^*}{(V^*)^2} \right) . \qquad \text{Equation 2-26.}$$

A copy of the source code for the calculation of the speed of sound using the truncated virial equation of state for argon is given in Appendix C.

The FFT was performed using the base 2 Cooley Tukey algorithm.[8] The base 2 algorithm was chosen to optimize the round off error. Although the base 3 algorithm has a more efficient Floating Point Operation (FLOP) count,[9] a digital computer, which also operates normally in base 2, preferentially accommodates calculations which use the base 2 number system. This then calls for the number of samples to be some integral power of 2. The operational bounds of the FFT are as follows:

The magnitude of the frequency domain is

$$n_f = \frac{n_s}{2} \quad \begin{Bmatrix} n_s = no.\ of\ samples \\ n_f = no.\ of\ frequencies \end{Bmatrix}; \qquad \text{Equation 2-27.}$$

the Nyquist limit of maximum frequency is

$$f_{max} = \frac{sample\ rate}{2}; \qquad \text{Equation 2-28.}$$

---

[8] J.W. Cooley and J.W. Tukey, "An Algorithm for the Machine Calculation of Complex Fourier Series," Mathematical Computations 19 (April 1965): 297-301.

[9] G.D. Bergland, "A Fast Fourier Transform Algorithm for Real-Valued Series," Communications of the ACM 11 (October 1968): 703-710.

the period for sampling is

$$\tau = \frac{n_s}{(sample\ rate)}; \qquad \text{Equation 2-29.}$$

the frequency resolution is

$$f_{res} = \frac{f_{max}}{n_f}; \qquad \text{Equation 2-30.}$$

and the FLOP count is

$$FLOP = n_s \log_2 n_s. \qquad \text{Equation 2-31.}$$

The ST was performed using the following algorithm

$$\begin{aligned} &denom = 2\pi g f_{res} \\ &For\ i = 1, n_{max} \\ &\quad ratio = \frac{c_i}{denom} \\ &\quad w_i = 0 \\ &\quad For\ j = 1, n_r \\ &\quad\quad index = integer(ratio * R_j) \\ &\quad\quad w_i = w_i + a_{index} \end{aligned} \qquad \text{Equation 2-32.}$$

The maximum speed is limited by insuring that all ST frequencies of the roots exist within the FFT frequency domain

$$c_{max} = \frac{f_{max} 2\pi g}{R_{n_r}}. \qquad \text{Equation 2-33.}$$

where n_r = number of roots in the truncated ST basis set. Since

$$\frac{c_{res}}{c_{max}} = \frac{f_{res}}{f_{max}}, \qquad \text{Equation 2-34.}$$

then the resolution of the algorithm and magnitude of the sonic domain are, respectively,

$$c_{res} = \frac{c_{max}}{n_{max}}, \quad n_{max} = \frac{c_{max}}{c_{res}} = n_f, \qquad \text{Equation 2-35.}$$

with a FLOP count of

$$FLOPs = n_{max} 2 n_r. \qquad \text{Equation 2-36.}$$

The theory of design is related to the construction of the apparatus in that building a very precisely known spherical cavity provides a geometry factor (g) that is simply the radius of the sphere. Once the geometry factor is known and an ADC is chosen, the rest of the parameters are fixed. For a given buffer size and sample rate, the frequency range and resolution are set; and for a given set of roots, the sonic range and resolution are set. The

selection of an ADC should consider the geometry of the apparatus as well as the sonic range of interest. In the next chapter the interfacing employing an ADC as well as the design of the apparatus are described.

CHAPTER 3
EXPERIMENTAL

The experimental design of this technique must address two principal problems, the computer interfacing of the data acquisition methods and the mechanical design of the apparatus. In a modern laboratory, data acquisition is no longer the tedious matter of turning dials, reading meters and logging data. Even the most impartial researcher tends to be inconsistent when manually measuring large amounts of data over long periods of time. The digital computer has taken over these more tedious tasks with much better speed and consistency. The first part of this chapter describes the interfacing of the computer involving data acquisition.

In addition, as more tasks are controlled by the computer, more time remains for the scientist to evaluate results and implement design improvements. Specifically during this work, volume control was added for the first time. Knowing the exact volume of the apparatus has always been necessary, but this volume has in the past been fixed. Many experiments, however, would benefit from a direct measurement of the effect of volume change. For example, $V^2(\partial P/\partial V)_T$ could be substituted into Equation 2-22 along with the speed of sound at zero frequency (c_0) and the

molecular weight (M) for a direct measurement of γ. To this end, an extremely accurate variable volume control was designed for this apparatus.

Interfacing

Data collection utilizes five basic devices and two computers. The physical parameters measured are temperature, equilibrium pressure, amplitude ($\propto$ acoustic pressure) and time. The first two of these measurements were made using standard laboratory instruments. Temperature is obtained by measuring the resistance of a platinum Resistance Temperature Device (RTD) using a Keithley 195a Digital Multi-Meter (DMM). The acquired resistance was updated and sent to the 8088 Central Processing Unit (CPU) along the National Instruments General Purpose Interface Bus (GPIB or IEEE) every 0.1 seconds. Resistance was then converted to temperature, in accordance with the RTD manufacturer's specifications, by the 8088 CPU. Pressure was read from a calibrated pressure sensitive Beckman Digital Strain Gauge in units of Pounds per Square Inch Absolute (PSIA). These readings were updated and sent to the CPU along the IEEE bus every 0.5 seconds.

Amplitude and time were measured simultaneously by the WAAG II Analog to Digital Converter (ADC). The WAAG ADC has eight-bit resolution, a 32768 point buffer and multiple sample rates of 40MHz, 4MHz, 400kHz, 40kHz and 4kHz. The

measurements are read and stored into the buffer sequentially. As a new measurement is added to the buffer, the oldest value is discarded. Once polled by the computer, the WAAG II dumps its entire buffer to the 8088 Random Access Memory (RAM) and then proceeds to acquire new data. The algorithm for the acquisition (source code provided in Appendix D) is as follows

```
For i-1,n
    r-resistance rtd
    T_i-convert(r)
    P-reading for strain guage
    amp-dump ADC buffer
    dump amp on hard drive
dump T on hard drive
dump P on hard drive
```

Equation 3-1.

Using Equation 2-28, a sample rate of 40kHz leads to a maximum frequency (f_{max}) of 20 kHz. With a buffer size of 32768, the period of sampling (τ) and frequency magnitude (n_f) were found from Equations 2-29 and 2-27, respectively, to be 0.8192 seconds and 16384. The resulting frequency resolution (f_{res}) from Equation 2-30 was approximately 1.22 Hz.

The excitation frequency is generated by a Hewlett Packard HP3325b function synthesizer. When the HP3325b is put into discrete sweep mode, it generates a frequency-

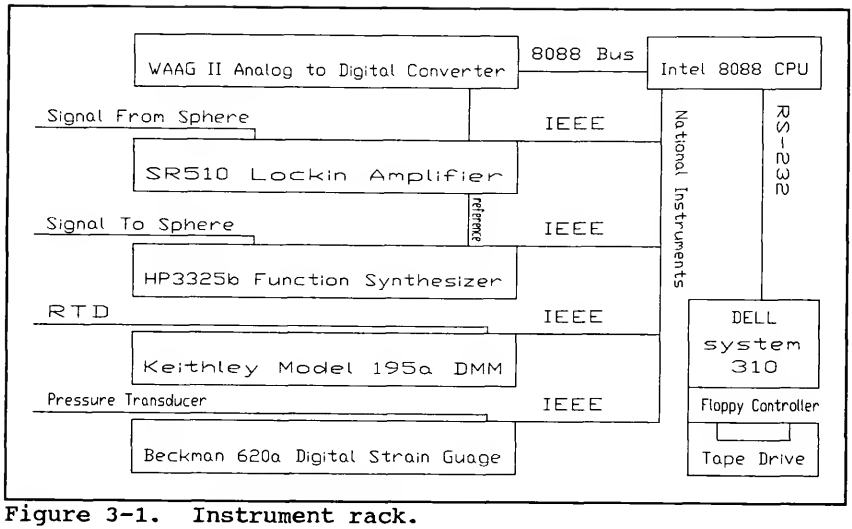

Figure 3-1. Instrument rack.

modulated-phase-consistent sinewave that sweeps from 0 Hz to 20 kHz in 0.8192 seconds, then repeats from 0Hz to 20kHz with a peak-to-peak voltage of 20.0 Volts. A TTL reference wave is sent to a Stanford Research SR510 lock-in amplifier from the HP3325b. The return signal from the resonator is also sent to the SR510, and all frequencies except for the reference frequency are filtered out by the frequency dependent band pass filter in the SR510. The resulting signal is then amplified and sent to the WAAG II ADC. All gain and power settings can be sent to the instruments along the IEEE bus.

The waveform collected by the ADC is dumped to hard drive in binary format while temperature and pressure are stored in an array but are later dumped to hard drive in binary format just before the program terminates. The

binary data are then sent to the DELL system 310 micro computer, the processing computer system. The binary format of the 8088 (8 bit) is different from the binary format of the DELL (32 bit), so the data must be translated to a common format. Since the data ranges in values from 0 to 255, two hexadecimal numbers can contain one datum (for source code, see Appendix E). The binary data are transformed to hexadecimal by the DELL then further transformed into the frequency domain.

Because the resulting large data set was limited to eight-bit resolution, a time correlation method was used to reduce floating point error. This method simply doubles the data set by adding the waveform to itself. It should be noted that this does not increase resolution by having a double basis set but simply lessens round off error of the computer; the frequency domain data are unaffected. The data are then dumped to the DELL hard drive. Data are then transformed to the sonic domain and dumped to the DELL hard drive in binary format (see Appendix B for source code). Three of the data sets--time domain 8088 binary format, frequency domain DELL binary format, and sonic domain DELL binary format--are then stored, along with all the source code used in the process, on tape. The process was then repeated for different temperatures.

Apparatus

The apparatus consists of four basic parts--the spherical cavity, the volume-controlling bellows, the reciprocating pump and the Delta Design series 9000 environmental chamber.

Spherical Cavity

The spherical cavity was constructed from two solid pieces of 303 stainless steel; a three-inch radius spherical cavity was cut from the center. Excess material was removed from the outer portion to lower the mass of the sphere thereby making it easier to control its temperature. To assure safe operation at the highest intended pressure (4000 PSIA), the minimum wall thickness was set at 6.4 mm (0.25 in). This dimension was based on a calculation of the bursting pressure in a spherical shell obtained by setting the force acting to stretch the walls equal to the tensile strength of the stainless steel. A safety factor of 4 was used.

The top portion of the sphere contains the two transducer mounts. A Macor insulated electrical feed-through was mounted by employing a customized tapered ram seal with annealed copper gaskets. The inner threaded portion was used to align the transducer. The transducers were Piezoelectric lead-Zirconate lead-Titanate (PZT) bimorphs which have high motion sensitivity. They were

placed as close as possible to the surface of the sphere in order to minimize departure from the sphericity. The two halves of the sphere were sealed together using an annealed copper gasket with a conflat type knife-edge seal and held together with two mild steel clamps as shown in Figure 3-2. Inlet ports for the gas were constructed on the top and bottom of the spherical cavity. The entire assembly was pressure tested to 3500 PSIA at room temperature.

Pump

The pump chamber (Figure 3-3) was constructed of a 304 stainless steel tube, 13 inches long with 1.250 inch outside diameter and 0.148 inch wall. The top portion was sealed by brazing a 304 stainless seal plug 1/2 inch thick with a 1/16 inch bore. The bottom portion was sealed by a 304 stainless steel plate with an annealed copper gasket on a conflat knife-edge seal. Seven magnetic field coils aligned concentrically on the tube create the pumping action by successively attracting a magnetic piston free to move inside the stainless steel tube. The bottom two coils are switched on remotely; the third coil from the bottom is activated as the bottom coil is turned off. This action is repeated until the magnetic piston reaches the top of the tube. Then a reversed action moves the magnetic piston to the bottom of the tube to complete one pumping cycle. Doubled-pumping action is created by use of four one-way

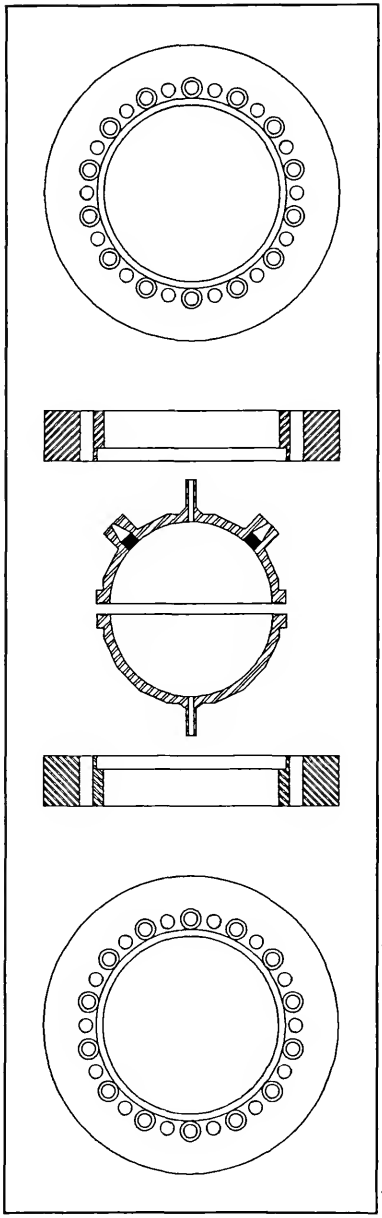

Figure 3-2. Spherical cavity sections and clamping flanges.

valves placed outside the assembly. The strength of the magnetic field as well as the frequency of field oscillation are adjusted remotely. At the highest field strength and frequency of oscillation, a pumping speed of 200 mL per second at room temperature and pressure was recorded. An aluminum mount was constructed to hold the pump in an upright position.

The Bellows

The addition of the bellows assembly brings on-line volume or density control to this technology for the first time. The collapsible bellows, constructed of 0.005 inch thick 304 stainless steel, was welded to a 1 inch thick plate which had a 1/4 inch hole bored horizontally to connect the adjustable volume of the bellows to the spherical cavity.

The outer portion of the bellows is contained in a chamber that was constructed from a solid piece of stainless steel and sealed to the lower plate with a triangular annealed copper seal[1]. The volume of the outer chamber was isolated from the spherical cavity and maintained at pressures slightly below (approximately 20 PSI) that of the spherical cavity. This then maintained the bellows in an expanded position. The volume of the bellows was controlled by a threaded ram bolted to the top of the outer chamber.

---

[1] Technology developed by S.O. Colgate in 1990.

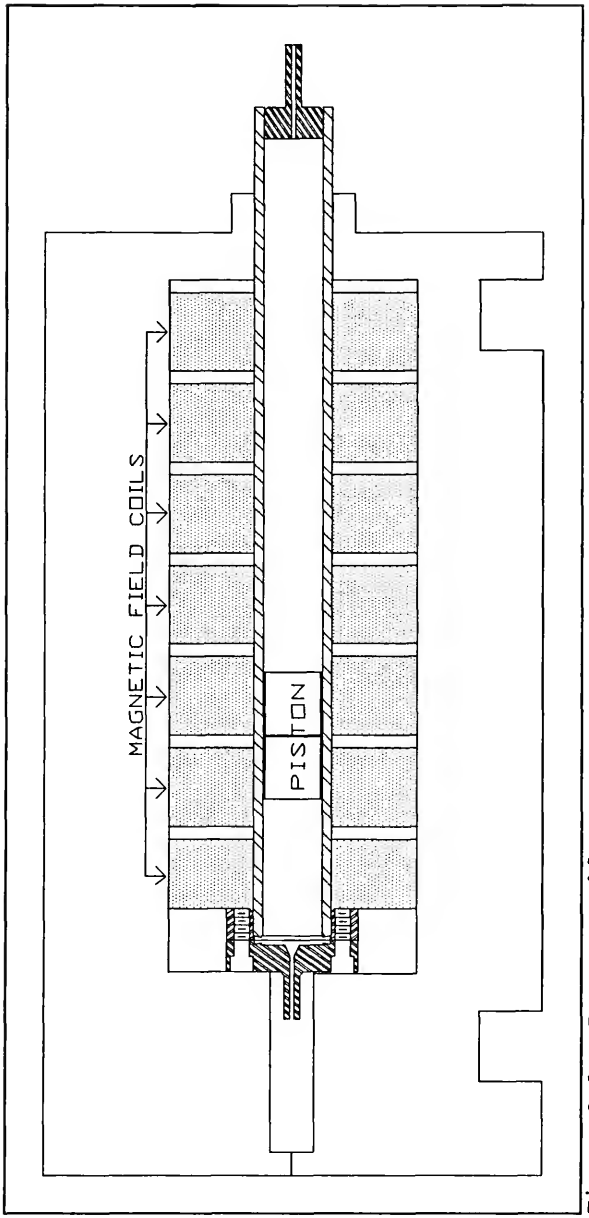

Figure 3-3. Pump assembly.

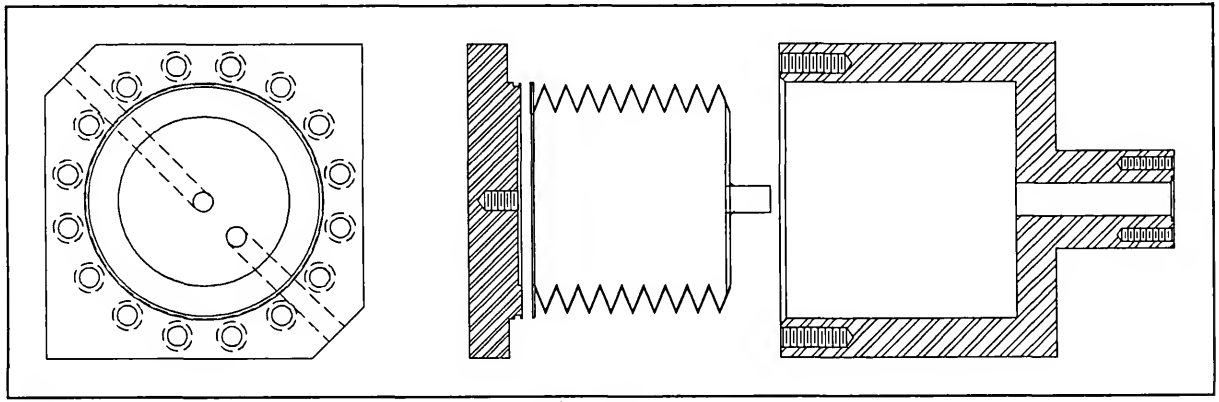

Figure 3-4. The bellows and bellows chamber.

The position of the ram was externally controlled by a customized micrometer to within 0.001 inch. The pressure was monitored by two Sensotec pressure transducers. The pressure transducers were not able to operate in the harsh conditions of the environmental chamber so they were placed outside the chamber and connected to the apparatus by two stainless steel capillary tubes. These capillary tubes prevented a large volume of the sample from being outside the temperature-controlled volume. The assembled apparatus was connected as shown in Figure 3-5.

The completely assembled apparatus was then placed into the environmental chamber. The environmental chamber operates over the temperature range of 150°C to -170°C and is controlled by the manufacturer's programming language sent along the IEEE bus. The assembled apparatus was pressure tested up to 2800 PSIA.

The calibrated apparatus presently requires that only one parameter, the volume, be monitored and controlled by the user. The other three state variables, temperature, pressure and speed of sound, are acquired automatically by the computer. Typical results are displayed in the next chapter.

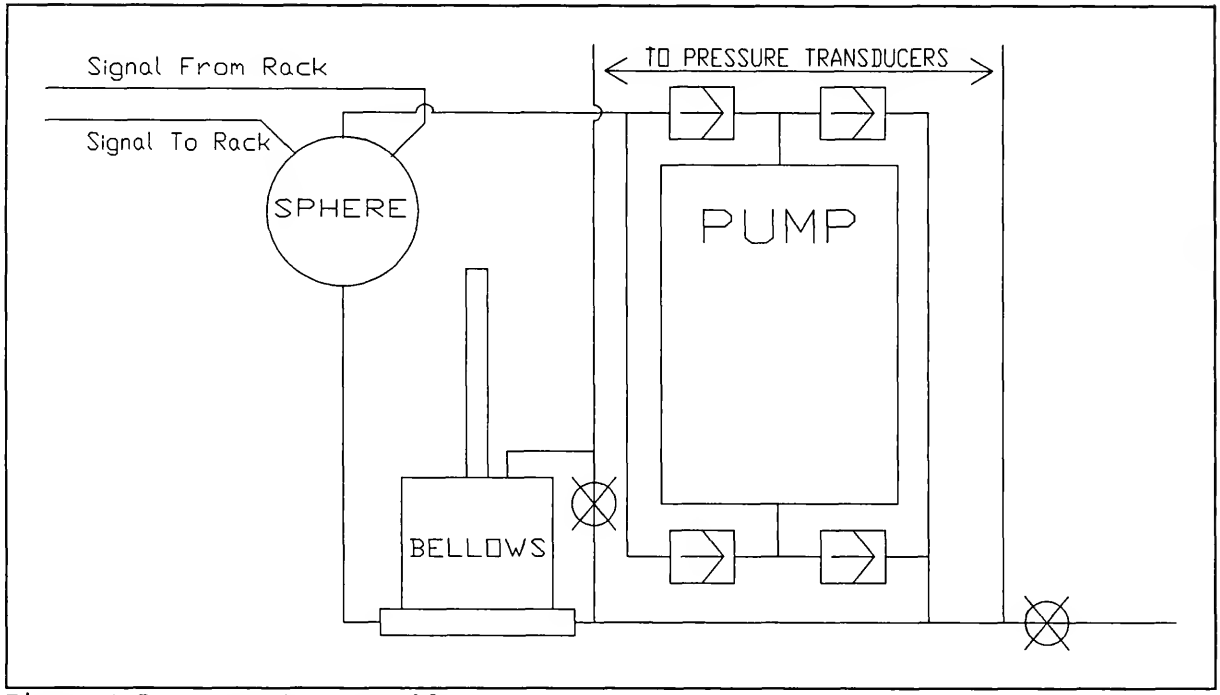

Figure 3-5. Apparatus assembly.

CHAPTER 4
DATA AND RESULTS

The data and plots resulting from this experiment are discussed in three groups. This includes a theoretical computer synthesized set of data, an experimentally acquired set of data for argon at low temperatures and then a discussion of argon at high temperatures.

Figure 4-1 depicts a theoretical waveform based on using the first 84 resonances in a spherical cavity (radius of 3 inches) filled with a fluid medium which propagates sound at 350 m/s. Figure 4-2 depicts a similar theoretical waveform again using the first 84 resonances in the same cavity but now containing a fluid medium which propagates a speed of sound at two speeds, 350 m/s and 150 m/s. These two waveforms simulate those which would be acquired by the ADC under ideal conditions.

Figure 4-3 depicts the FFT of the waveform shown in Figure 4-1 while Figure 4-4 depicts the FFT of the waveform shown in Figure 4-2. Figure 4-5 displays the final results of the ST of the FFT described in Figure 4-3 and Figure 4-6 displays the results of the ST of the FFT in Figure 4-4. These six figures portray the chronological order of acquisition and calculation for the simulated set of data.

Note that ST transforms shown in Figures 4-5 and 4-6 correctly recover the input sonic speeds (350 m/s and 150 m/s).

Figure 4-7 is an experimentally acquired waveform of the resonances of argon at a low temperature (-31.56°C) in a spherical cavity with a 3.000 inch radius. The experimental conditions are given in Table 4-1. An expanded view of a section of Figure 4-7 is given in Figure 4-8 to show the resolution with which the waveform is acquired in other regions. The FFT of the waveform of Figure 4-7 is shown in Figure 4-9 and the relevant physical and computational parameters are given in Table 4-2. As seen in Figure 4-9, the baseline is not very stable in the region of 10,000 Hz. An expanded view of this region is shown in Figure 4-10. Several STs were performed on the data in Figure 4-9 using different numbers of roots. The resulting ST weights employing the first 21 roots are shown in Figure 4-11 with an expanded view of the region that contains the known speed of sound in argon shown in Figure 4-12. The experimental and computational parameters are given in Table 4-3. Four STs were performed on the same FFT data in which only the number of roots used in the ST were changed. The results are shown in Figures 4-11 through 4-18 while parameters are listed in Tables 4-3 through 4-6. These results reveal the important features of the technique; they are described later in this chapter.

The same experiment was performed at a higher temperature (50.93°C). Figure 4-19 shows the experimentally acquired waveform with the experimental and computational parameters given in Table 4-7. The expanded view shown in Figure 4-20 indicates that more of the resolution of the ADC was utilized. The baseline of the FFT shown in Figure 4-21 is considerably better than that of the low temperature experiment (Figure 4-9). The expanded view shown in Figure 4-22 indicates that the sharp acoustic resonances are larger than the perturbed baseline and are better resolved than those in Figure 4-10. The four STs using the different sets of basis functions at this temperature are shown in Figures 4-23 through 4-30 along with the corresponding parameters in Tables 4-9 through 4-12.

Interpretations of the data and graphs presented above are organized as follows. The first section discusses the characteristics of the time domain signal and how it deviates from ideality. The second discusses the characteristics of the frequency domain while the third section examines the sonic domain and the influence of varying the number of roots (n_r). In addition, the volume calibration data are included at the end of the chapter.

Time Domain Plots

Figures 4-1 and 4-2 show two computer simulated ADC signals. Figure 4-1 was generated from the sum of 84

sinewaves with frequencies generated from Equation 2-11 for a sonic speed (c) of 350 m/s, a geometric factor (g) of 3 inches and assuming equal amplitudes of the resonances. Figure 4-2 was generated from two sets of 84 sinewaves--one for c = 150 m/s, the other for c = 350 m/s. Both waveforms are similar in that they show no beat patterns or interference. Figure 4-7 shows a low temperature ADC signal where the resolution is quite low except for when the excitation frequency corresponds closely to a resonance frequency. This is an indication that the resonances are decaying rapidly. Figure 4-19 shows a high temperature ADC signal where the resolution is better since clearly the resonances are not decaying as rapidly as in the low temperature case. In other words, Figure 4-19 is approaching the characteristic of Figures 4-1 and 4-2. Ideally, an evenly distributed waveform uses the entire resolution of the ADC as was seen in the expanded Figures 4-8 and 4-20; that is not the case here. The resolution acquired is less than half the ADC resolution.

Frequency Domain Plots

The baselines of the frequency domain plots in Figures 4-3 and 4-4 indicate that the amplitudes are perturbed due to floating point calculation error. The low temperature frequency domain plot in Figure 4-9 shows an extremely large broad peak in the center of the frequency spectrum. The

expanded view shown in Figure 4-10, however, shows the sharp gas resonances imposed on top of this large peak. As the temperature is increased and the decaying of the resonances decreases, the broad peak decreases in size as well as frequency. All of these characteristics indicate that this portion of the signal is associated with vibrations of a solid, perhaps along the walls of the sphere or in the transducers themselves.

Sonic Domain Plots

The two sonic domain plots in Figures 4-5 and 4-6 indicate that the amplitude perturbations of the frequency domain do not affect the amplitudes in the sonic domain, but that much of the floating point calculation noise is carried through. The plots do show that the ST will resolve multiple speeds of sound if present in the data, although all of the low and high temperature plots shown in the remaining figures have considerably different baselines. The baselines are attributed to the reproducible apparatus frequencies which are not due to normal mode vibrations of the cavity fluid. These are called nonacoustic frequencies. The reason that they are identifiable as being nonacoustic is that they do not move across the baseline as the basis set of roots is changed. The four low temperature figures (4-11 to 4-18) as well as the four high temperature figures (4-19 to 4-30) show that the baseline maps predominately

with respect to index and not speed. Only resonances that are acoustic will be speed dependent and not index dependent. As the absorption of energy by the gas increases in the high temperature spectra, the amplitude of the speed of sound begins to predominate as would be expected. It should be recalled here that the time domain signal is the same for all sonic domain plots of a given temperature; the only thing that was changed was the number roots used to form the basis. In addition, the size of the basis did not seem to have a large effect on the resolution. It was not until $n_r = 63$ that the resolution saw any significant increase, but this could be due to where the resonance was with respect to the noise and does not necessarily reflect an increase in gain.

The speeds of sound in argon calculated from the truncated virial equation (see Appendix C) are 291.644 m/s for the low temperature data (@ -31.56°C and 870.5 PSIA) and 350.245 m/s for the high temperature data (@ 50.93°C and 1285.5 PSIA). The ST speeds of sound are given in Tables 4-1 through 4-12. The ST basis assumes a perfect sphere with a radius of 3 inches. Even using this simplification, the ST method gives sonic speeds within less than 0.5% deviation from the calculated values. The other three physical measurements (temperature, pressure and volume) employed standard techniques and were calibrated as discussed in the next section.

Volume and Pressure Calibration

The volume and pressure calibration required two standard devices. For the pressure calibration, a Ruska Model 2465 Dead Weight Pressure Gauge was used. The accuracy of the Ruska gauge was ± 0.001 PSIA with a range from 0.000 PSIA to 650.000 PSIA. For the volume calibration, the Ruska gauge as well as a Ruska Model 25652 volumetric pump was used. The accuracy of the Ruska pump was ± 0.01 mL. The actual calibration of the Sensotec pressure transducers was the three point calibration described in the Beckman 620 owner's manual. The three pressures chosen were 0.000 PSIA, 320.000 PSIA and 640.000 PSIA. Since the accuracy of the Sensotec pressure transducers was only ± 0.5 PSIA, the accuracy of the three calibration pressures was more than necessary.

The volume calibration involved taking several volume and pressure measurements and employing the ideal gas equation to deduce the absolute volume as shown below

$$P_0 V_0 = P_i (V_0 + \Delta V_i)$$

$$\frac{P_i \Delta V_i}{P_0} = V_0 - V_0 \frac{P_i}{P_0} \quad , \qquad \text{Equation 4-1.}$$

where P_0 is the initial pressure and V_0 is the total volume of the apparatus at that pressure. P_i and ΔV_i are measured by the Ruska gauge and pump, respectively. The outside

volume of the calibration equipment was found from the data in Figure 4-31. The total volume of the apparatus as well as the calibration equipment was then found from the data in Figure 4-32. The volumes were all compared to a common point on the Ruska pump since the pump has its own volume that must be considered. The outside volume of the calibration equipment was then subtracted from the combined total to obtain the true total volume of the apparatus. Once the total volume was found, the change in volume due to the bellows from the same common point was found from the data in Figure 4-33. The change in volume with respect to the change in length of the external adjustment ram was observed to correlate best to a second order polynomial fit. The result (Table 4-15) was an expression for the total volume of the apparatus as a function of the external ram setting. The uncertainty in a total volume for a given ram setting was 0.01%. The range of the total volume of the apparatus was from 2350.00 to 2878.00 mL.

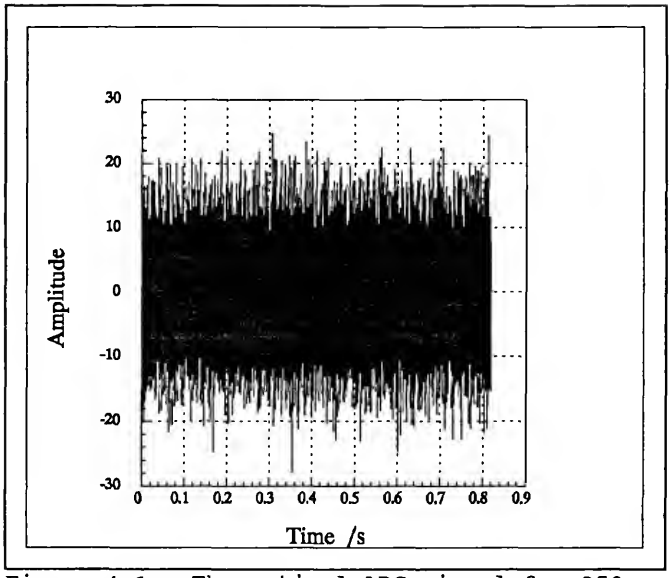

Figure 4-1. Theoretical ADC signal for 350 m/s of speed of sound.

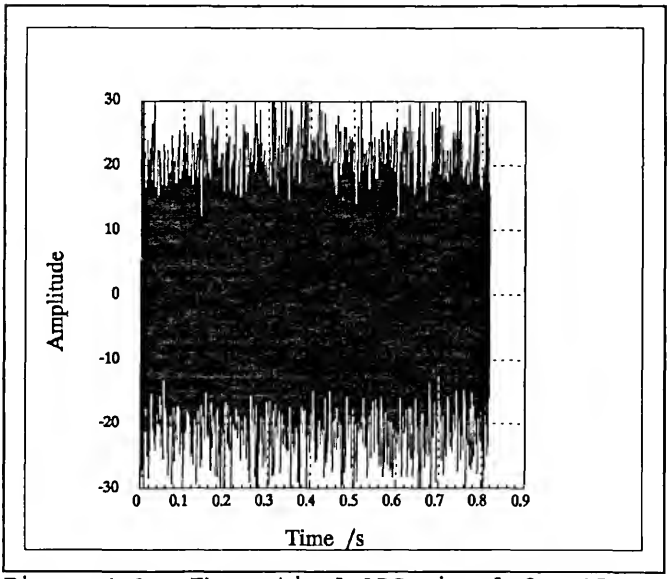

Figure 4-2. Theoretical ADC signal for 150 m/s and 350 m/s speeds of sound.

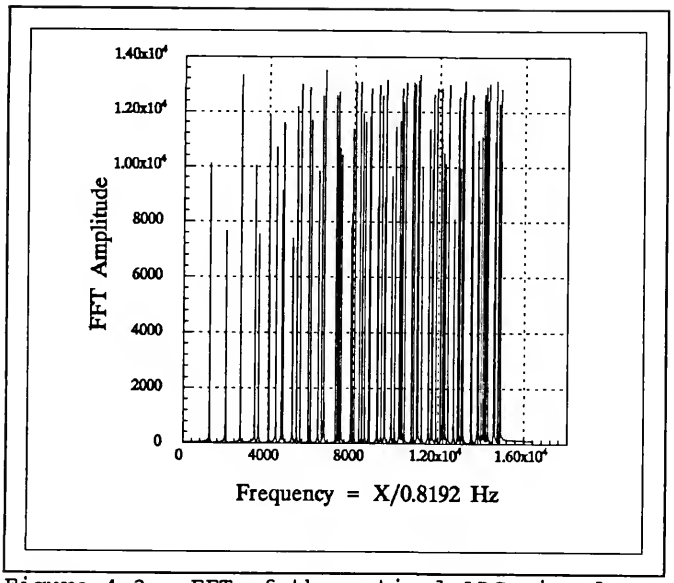

Figure 4-3. FFT of theoretical ADC signal for 350 m/s speed of sound.

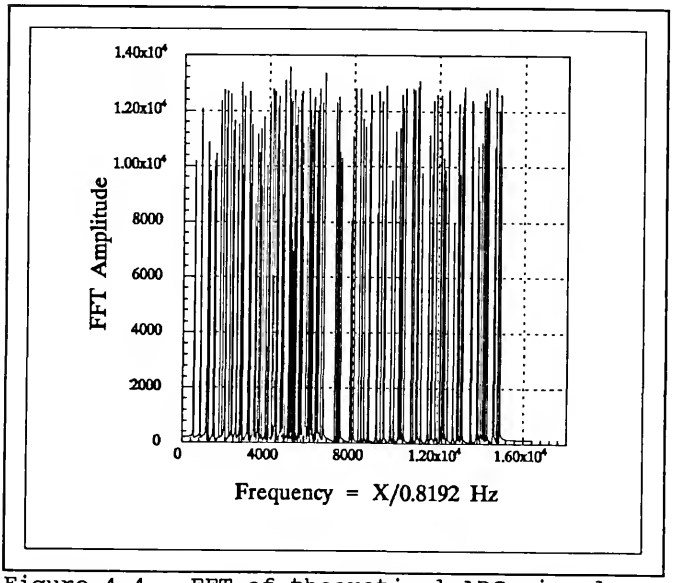

Figure 4-4. FFT of theoretical ADC signal for 150 m/s and 350 m/s speeds of sound.

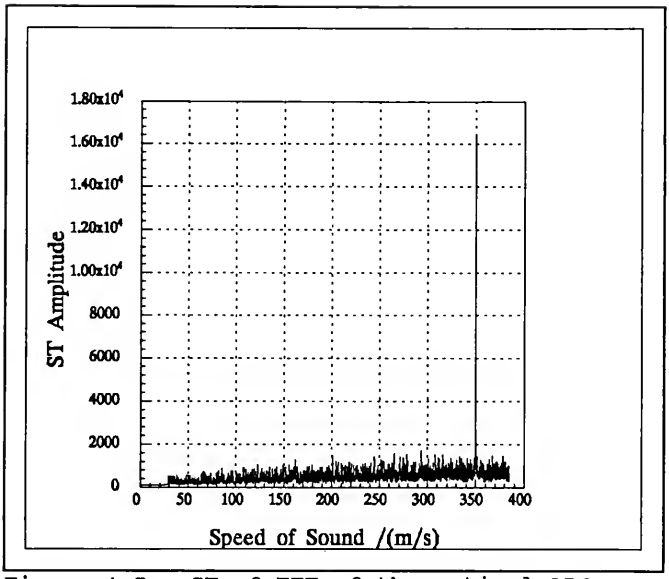

Figure 4-5. ST of FFT of theoretical ADC signal for 350 m/s.

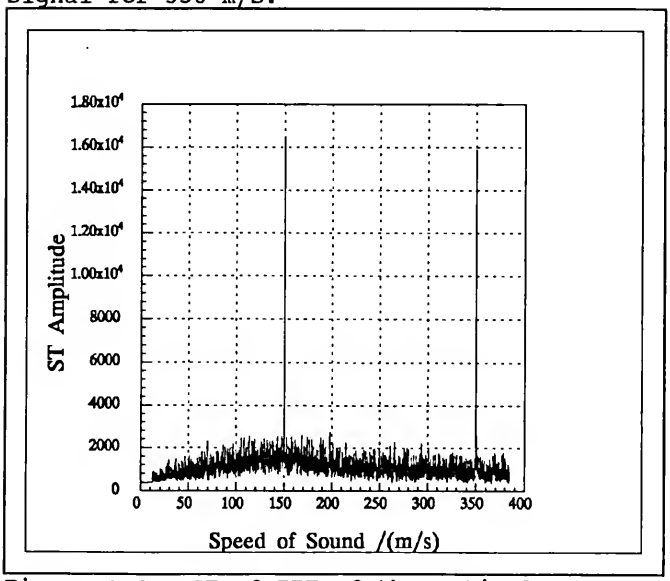

Figure 4-6. ST of FFT of theoretical ADC signal for 150 m/s and 350 m/s speeds of sound.

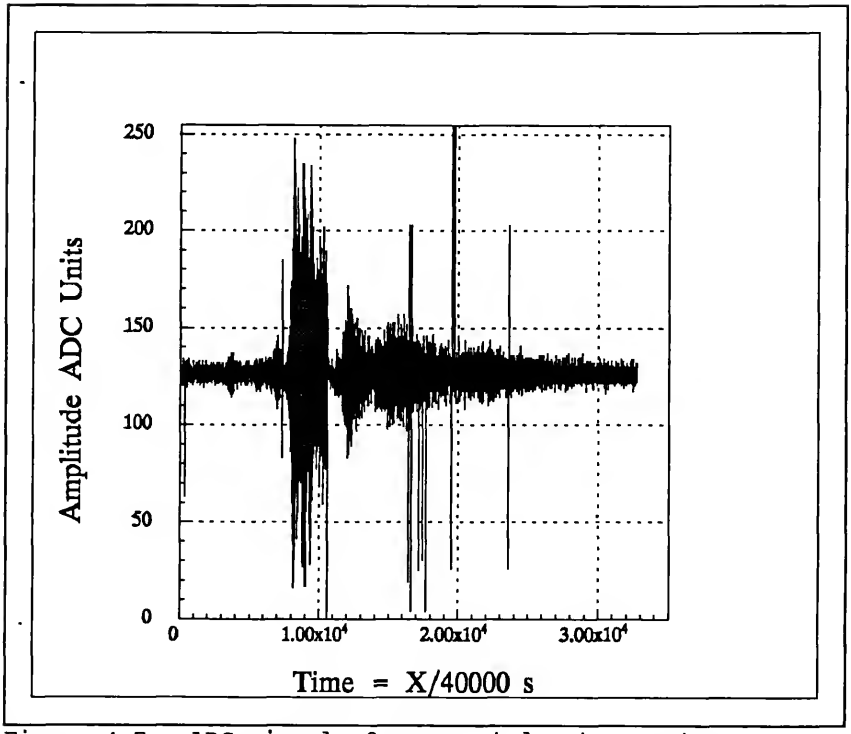

Figure 4-7. ADC signal of argon at low temperature.

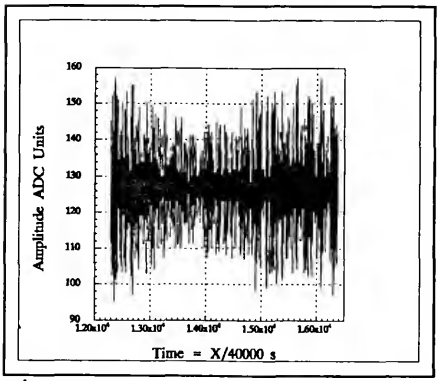

Figure 4-8. Expanded section of Figure 4-7.

Table 4-1. Low temperature time domain parameters of argon.

T = -31.56 ± .10°C

P = 870.5 ± .5 PSIA

n_s = 32768

Sample rate = 40 kHz

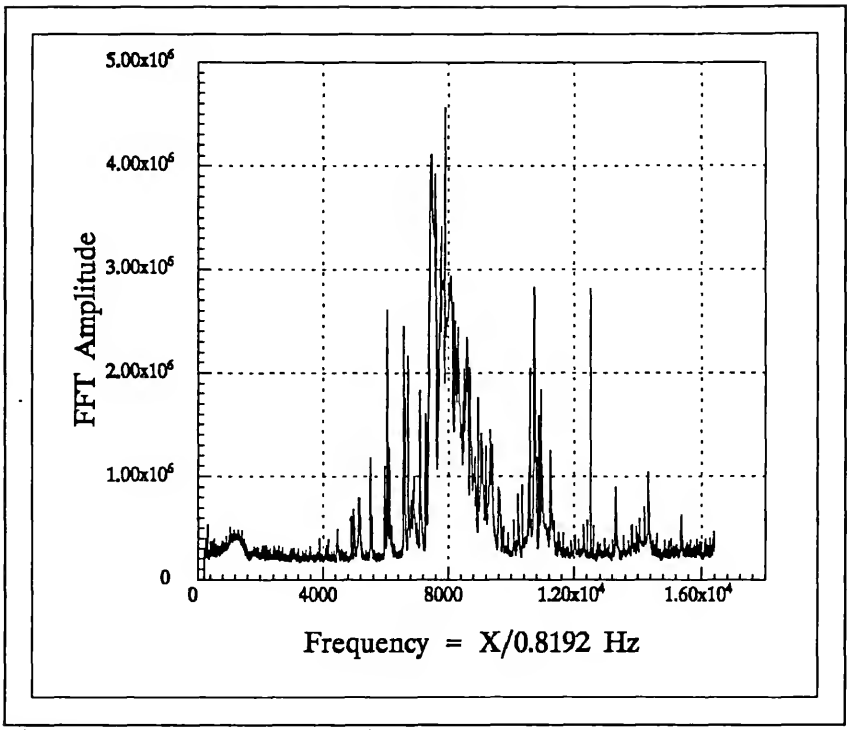

Figure 4-9. FFT of ADC signal of argon at low temperature.

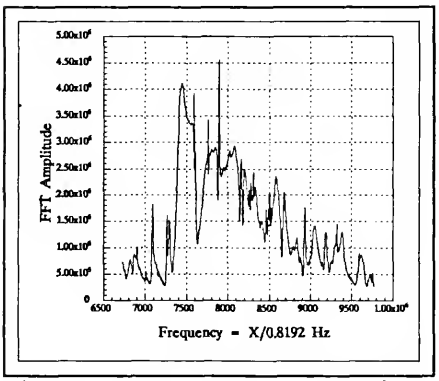

Figure 4-10. Expanded section of Figure 4-9.

Table 4-2. Low temperature frequency domain parameters of argon.

T = -31.56 ± .10°C

P = 870.5 ± .5 PSIA

n_f = 16384

f_{max} = 20 kHz

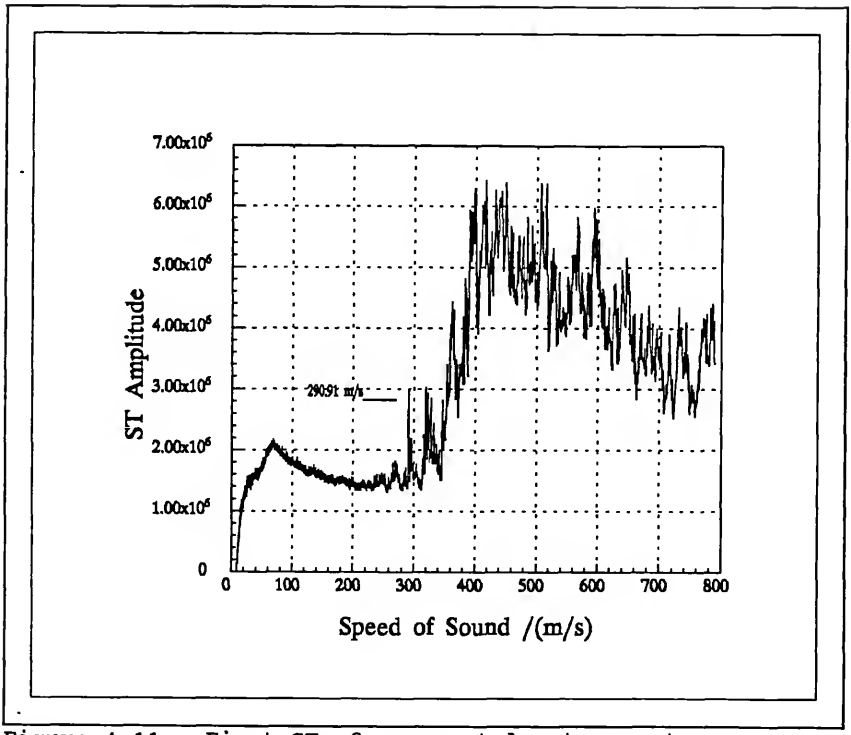

Figure 4-11. First ST of argon at low temperature.

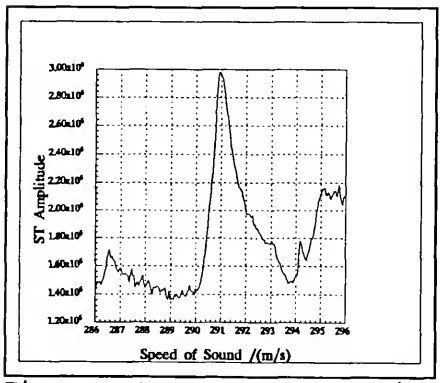

Figure 4-12. Expanded section of Figure 4-11.

Table 4-3. First sonic domain parameters of argon at low temperature.

T = -31.56 ± .10°C
P = 870.5 ± .5 PSIA
c = 290.91 ± .05 m/s
c_{max} = 788.532 m/s

n_r = 21

Note: See Equations 2-33, 2-35.

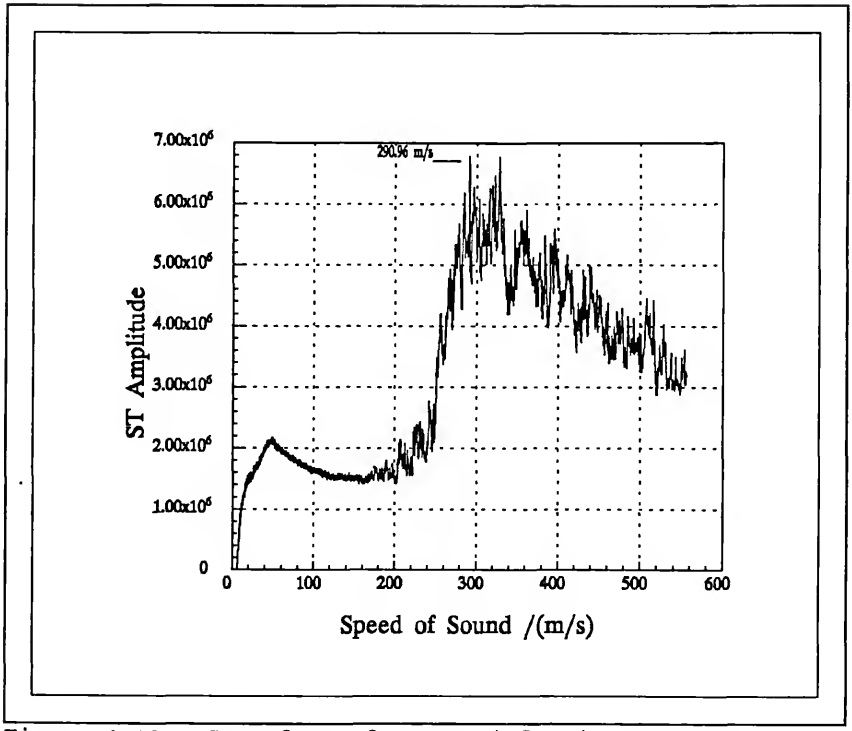

Figure 4-13. Second ST of argon at low temperature.

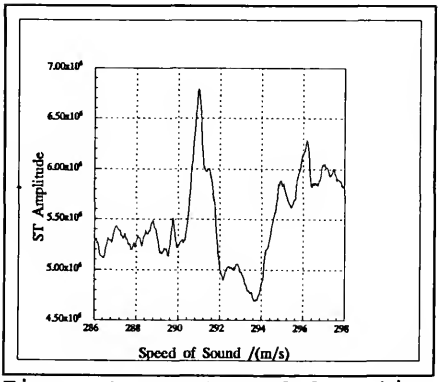

Figure 4-14. Expanded section of Figure 4-13.

Table 4-4. Second sonic domain parameters of argon at low temperature.

T = −31.56 ± .10°C
P = 870.5 ± .5 PSIA
c = 290.96 ± .03 m/s
c_{max} = 556.016 m/s

n_r = 42

Note: See Equations 2-33, 2-35.

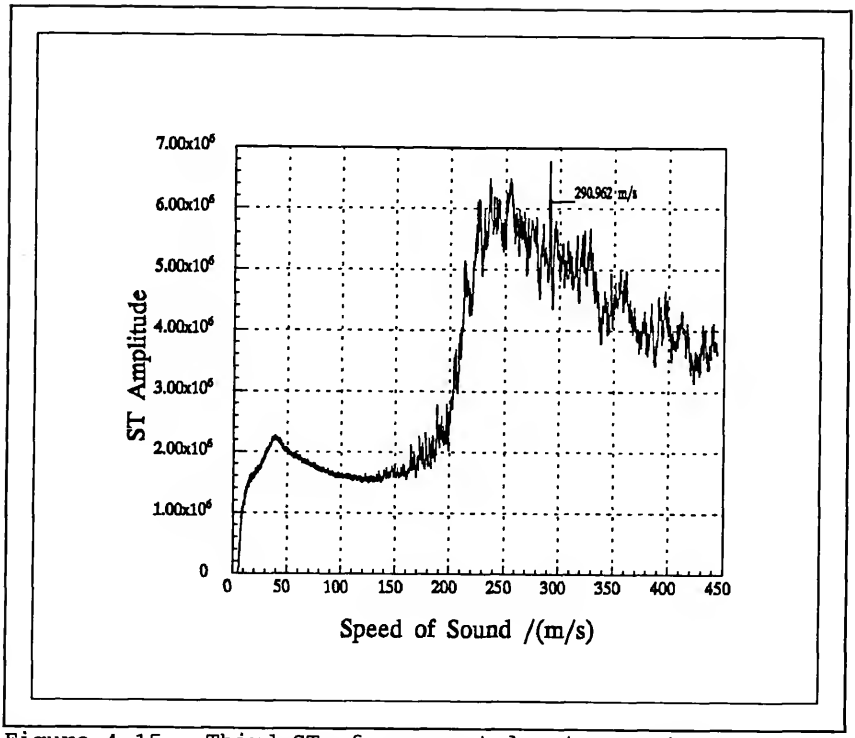

Figure 4-15. Third ST of argon at low temperature.

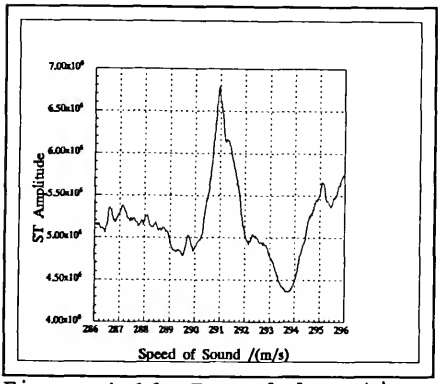

Figure 4-16. Expanded section of Figure 4-15.

Table 4-5. Third sonic domain parameters of argon at low temperature.

$T = -31.56 \pm .10°C$
$P = 870.5 \pm .5$ PSIA
$c = 290.962 \pm .027$ m/s
$c_{max} = 443.741$ m/s

$n_r = 63$

Note: See Equations 2-33, 2-35.

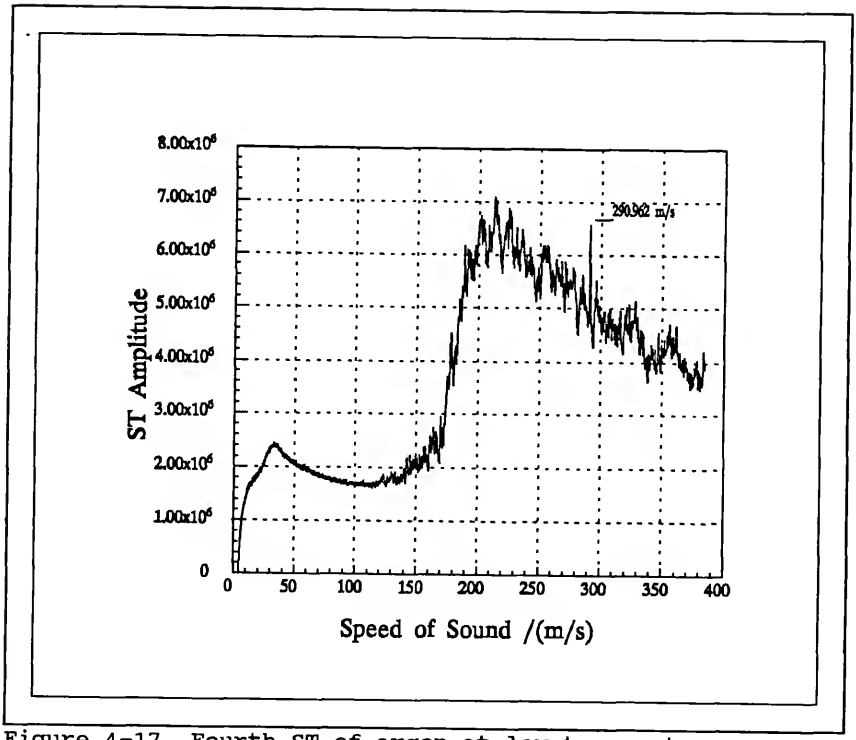

Figure 4-17. Fourth ST of argon at low temperature.

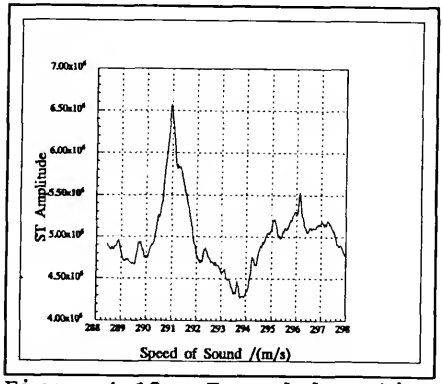

Figure 4-18. Expanded section of Figure 4-17.

Table 4-6. Fourth sonic domain parameters of argon at low temperature.

T = -31.56 ± .10°C
P = 870.5 ± .5 PSIA
c = 290.962 ± .023 m/s
c_{max} = 384.545 m/s

n_r = 84

Note: See Equations 2-33, 2-35.

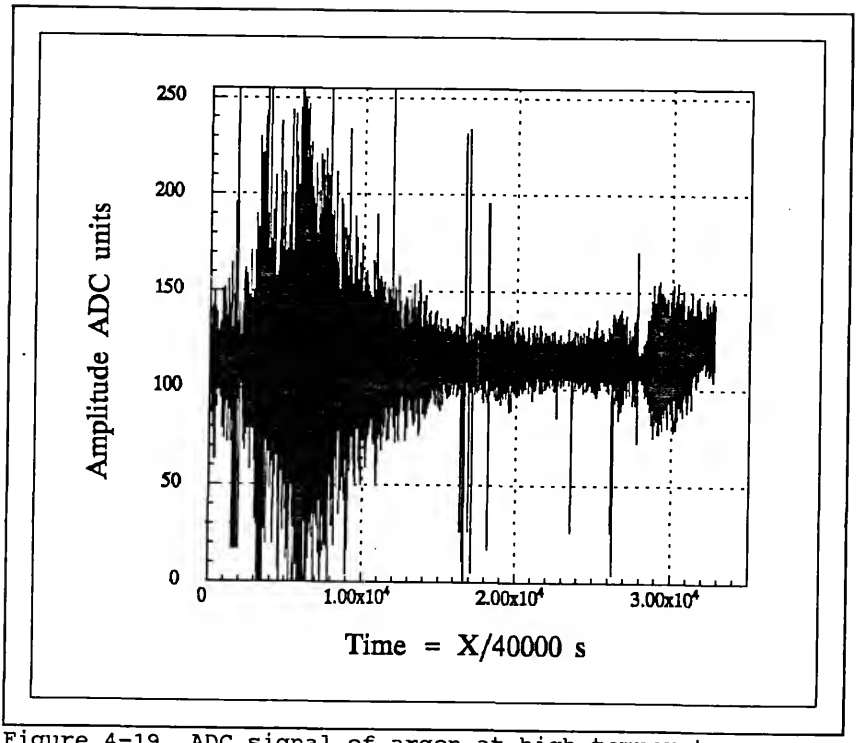

Figure 4-19. ADC signal of argon at high temperature.

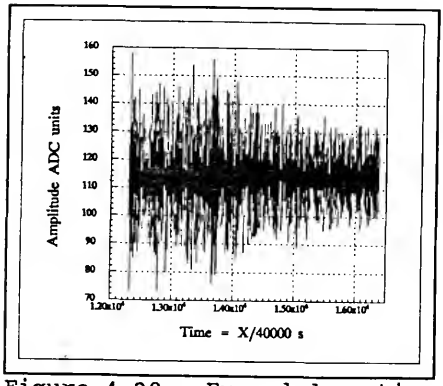

Figure 4-20. Expanded section of Figure 4-19.

Table 4-7. High temperature time domain parameters of argon.

T = 50.93 ± .06°C

P = 1285.5 ± .8 PSIA

n_s = 32768

Sample rate = 40 kHz

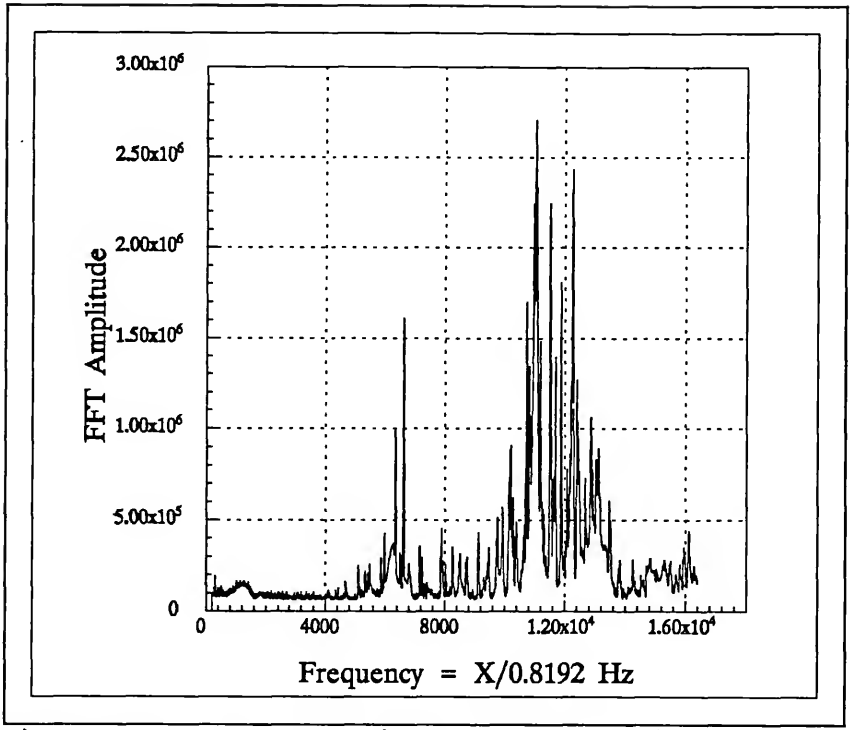

Figure 4-21. FFT of ADC signal of argon at high temperature.

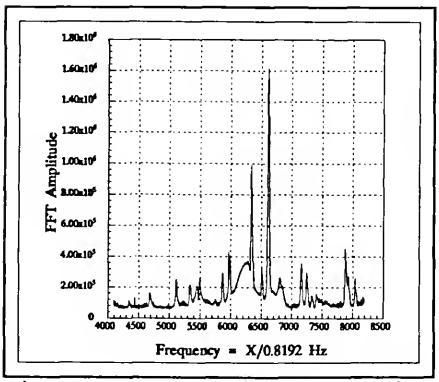

Figure 4-22. Expanded section of Figure 4-21.

Table 4-8. High temperature frequency domain parameters of argon.

T =	50.93 ± .06°C
P =	1285.5 ± .8 PSIA
n_f =	16384
f_{max} =	20 kHz

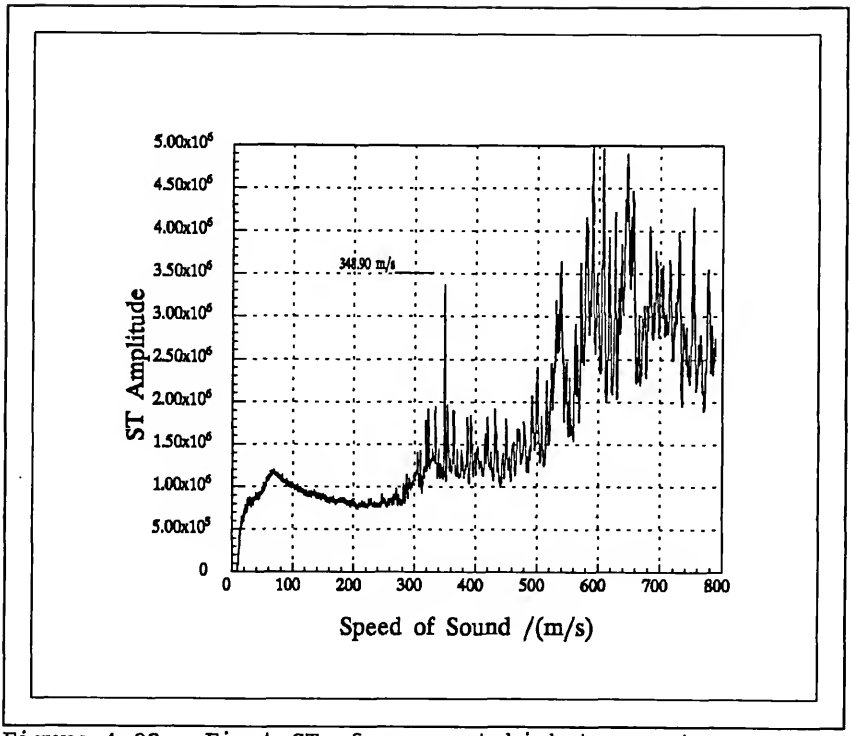

Figure 4-23. First ST of argon at high temperature.

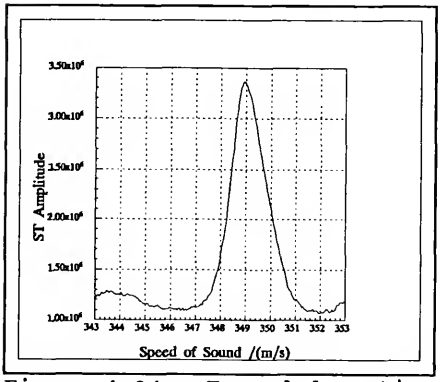

Figure 4-24. Expanded section of Figure 4-23.

Table 4-9. First sonic domain parameters of argon at high temperature.

T = 50.93 ± .06°C
P = 1285.5 ± .8 PSIA
c = 348.90 ± .05 m/s
c_{max} = 788.532 m/s

n_r = 21

Note: See Equations 2-33, 2-35.

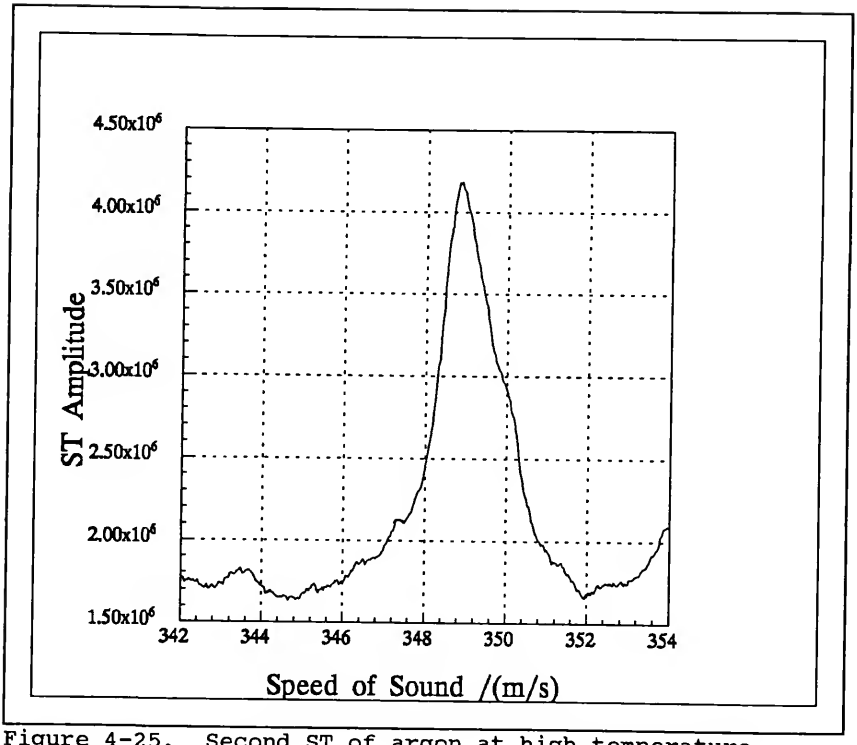

Figure 4-25. Second ST of argon at high temperature.

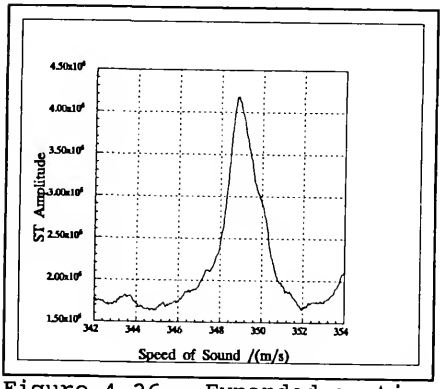

Figure 4-26. Expanded section of Figure 4-25.

Table 4-10. Second sonic domain parameters of argon at high temperature.

T = 50.93 ± .06°C
P = 1285.5 ± .8 PSIA
c = 348.79 ± .03 m/s
c_{max} = 556.016 m/s

n_r = 42

Note: See Equations 2-33, 2-35.

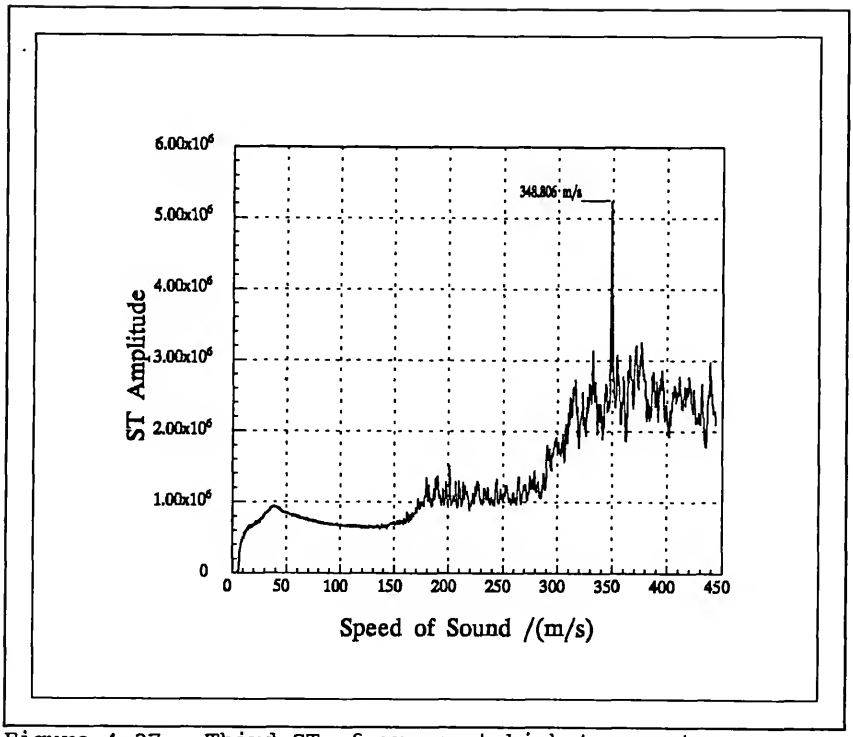

Figure 4-27. Third ST of argon at high temperature.

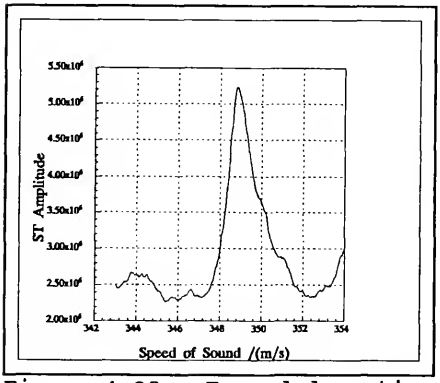

Figure 4-28. Expanded section of Figure 4-27.

Table 4-11. Third sonic domain parameters of argon at high temperature.

T = 50.93 ± .06°C
P = 1285.5 ± .8 PSIA
c = 348.806 ± .027 m/s
c_{max} = 443.741 m/s

n_r = 63

Note: See Equations 2-33, 2-35.

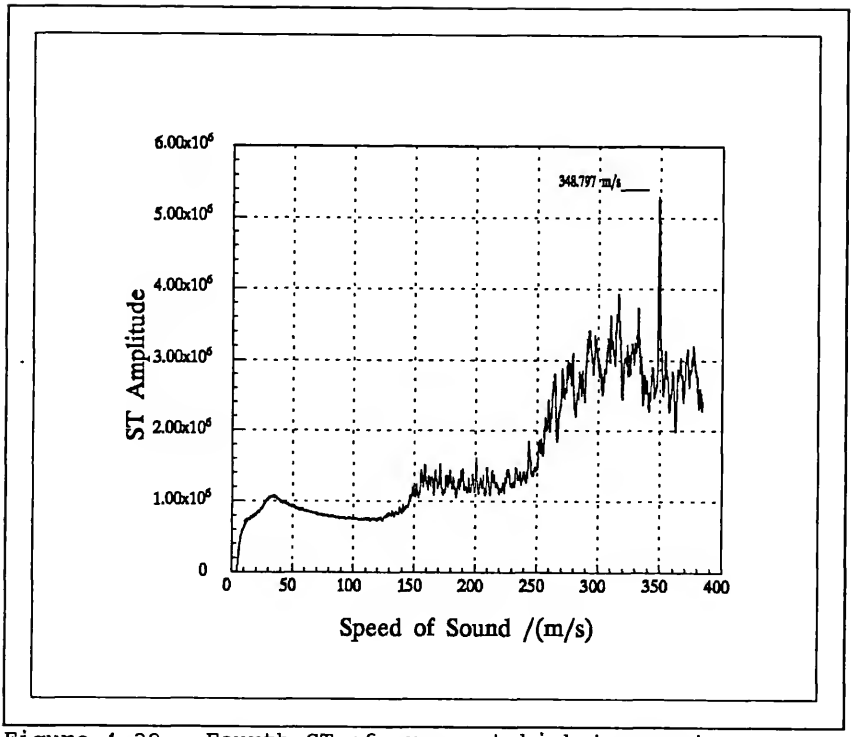

Figure 4-29. Fourth ST of argon at high temperature.

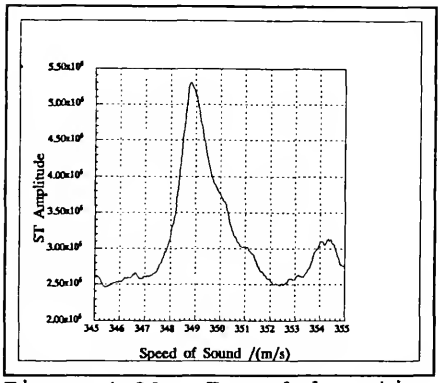

Figure 4-30. Expanded section of Figure 4-29.

Table 4-12. Fourth sonic domain parameters of argon at high temperature.

T = 50.93 ± .06°C
P = 1285.5 ± .8 PSIA
c = 348.797 ± .023 m/s
c_{max} = 384.545 m/s

n_r = 84

Note: See Equations 2-33, 2-35.

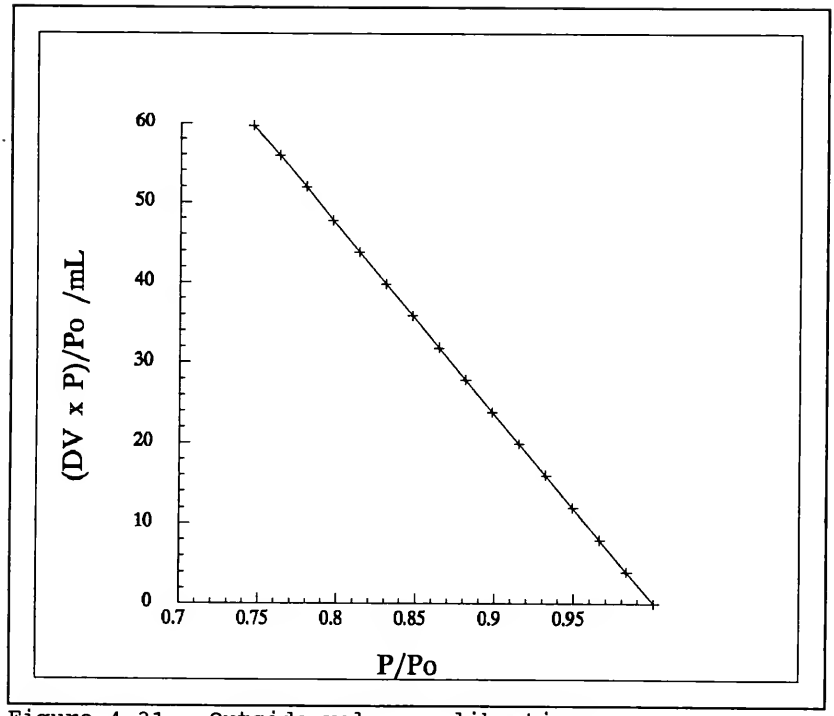

Figure 4-31. Outside volume calibration.

Table 4-13. Outside volume calibration.

slope = -235.074 mL

intercept = 235.0671 mL

V = 235.071 ± .007 mL

V_{250} = 100.953 ± .007 mL

correlation coefficient = 0.9999945

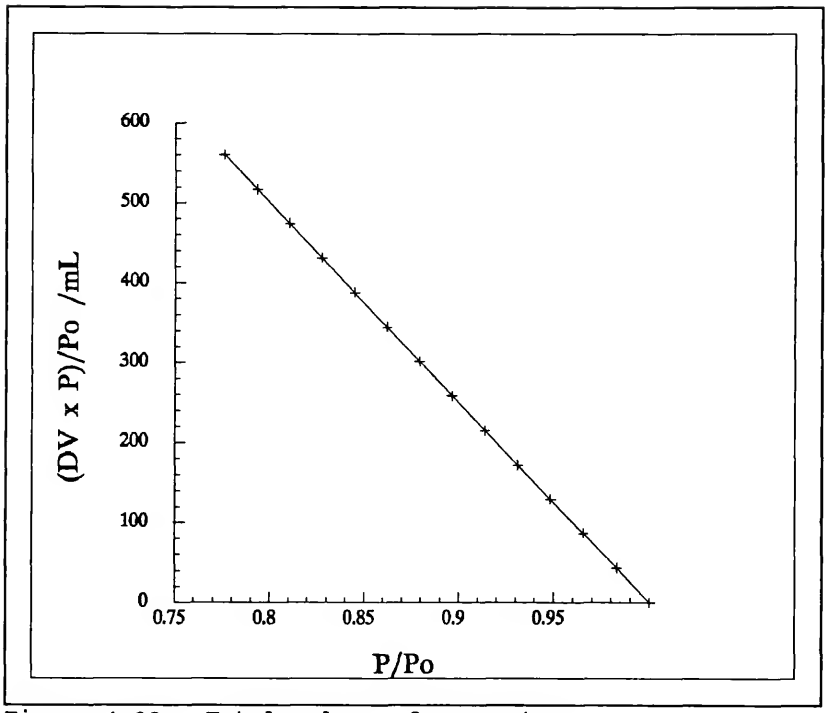

Figure 4-32. Total volume of apparatus.

Table 4-14. Total volume of apparatus.

slope = -2498.55 mL

intercept = 2498.517 mL

V = 2498.54 ± .03 mL

V_{250} = 2463.82 ± .03 mL

V_t = 2362.87 ± .03 mL at L = .250 inches

correlation coefficient = .999999

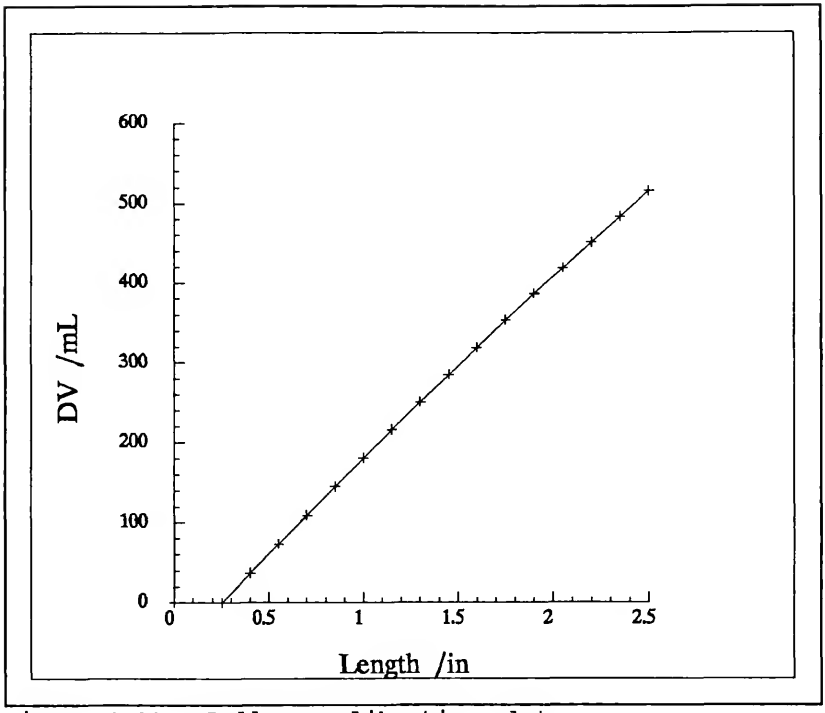

Figure 4-33. Bellows calibration plot.

Table 4-15. Bellows volume calibration.

First order coefficient = 251.60 ± 0.25 mL/in

Second order coefficient = -8.25 ± 0.10 mL/in^2

$V_t = 2300.19 + 251.60\ L - 8.25\ L^2$

Correlation coefficient = .999999

Table 4-16. Compiled results of sonic speeds of argon at low and high temperatures for various roots.

Speed $(m/s)^{-1}$	No. of Roots	Other Parameters
- - - - - - - - Low Temperature- - - - - - - - - - - - -		
290.91 ± .05	21	T = -31.56 ± .10°C
290.96 ± .03	42	P = 870.5 ± .5 PSIA
290.962 ± .027	63	LJ 6-12 speed of sound
290.962 ± .023	84	c = 291.644 m/s
		% difference = 0.2
- - - - - - - - High Temperature- - - - - - - - - - - - -		
348.90 ± .05	21	T = 50.93 ± .06°C
348.79 ± .03	42	P = 1285.5 ± .8 PSIA
348.806 ± .027	63	LJ 6-12 speed of sound
348.797 ± .023	84	c = 350.245 m/s
		% difference = 0.4

CHAPTER 5
CONCLUSION

From the results in Figures 4-5 and 4-6, one sees that the ST can correctly resolve the speed of sound or speeds of sound in an idealized spherical acoustic cavity. The identifiable speed of sound in Figure 4-5 is 350.000 m/s which is precisely the speed used to develop the time domain signal. In Figure 4-6, the identifiable speeds of sound were 150.000 m/s and 350.000 m/s which also matched precisely the speeds used to calculate the time domain signal. As discussed previously in the introduction, this transform assumes that there is no frequency dependence on the speed of sound. The speed that has thermodynamic significance as seen in Equation 2-22 is the speed of sound at zero frequency. This speed can be calculated by using the speed from the ST to identify the frequencies. Once these are identified and measured precisely, the speed at each frequency can be calculated by rearrangement of Equation 2-10 and a plot of speed vs. frequency can be developed. Extrapolation of this data to zero frequency will reveal the thermodynamically significant speed of sound at zero frequency.

This still does not account for the precondensation effects with the walls of the cavity.[1] Precondensation effects will also show up in the frequency domain. The actual magnitude of this effect can be very accurately investigated once the data are acquired. Although, the most accurate method of determining the speed of sound at zero frequency is still not certain, the present method is the first step to complete automation of this measurement. Even with no analysis or calibration (see Table 4-16), the ST speed of sound obtained from measurements on argon is within 0.5% of the calculated thermodynamic speed of sound at zero frequency.

The ST baseline for the experimental data had considerable noise due to the assumption made in Equation 2-12 that all frequencies detected by the FFT are acoustic. Clearly the baseline represents nonacoustic resonances of some kind. There are, of course, several ways to reduce this problem by increasing the gain of the acoustic frequencies. One way would involve isolating the transducers from any contact with the cavity and acoustically insulating the outer portion of the sphere. Another method would be to excite the acoustic frequencies selectively; or, in other words, perform an inverse ST to produce an arbitrary waveform that could be sent to the

---

[1] Mehl and Moldover, "Precondensation Phenomena in Acoustic Measurements."

driving transducer by a Digital to Analog Converter (DAC). By coupling the ADC signal to the waveform produced by the DAC, a sonic sweep could be performed where the arbitrary wave is swept over a sonic range and the sonic speed spectrum recorded. This would be analogous to the frequency swept method used in the past.

Even without resorting to the use of methods to enhance the baseline of the sonic spectrum, it is apparent from consideration of Figures 4-23 through 4-30 that the speed of sound can be expeditiously deduced with this technique. The time of acquisition is approximately 10 seconds with the equipment used in this experiment; thus, technically this is not a real time measurement. Bear in mind, however, that the acquisition was performed with an 8088 CPU (8 bit) computer. If a larger and faster computer were used, such as an 80386 (32 bit) computer, the total time of processing would be slightly more than the time of acquisition or approximately 1 second. By decreasing the sonic resolution, even shorter acquisition times could be achieved. These would then be comparable to the acquisition times of temperature and pressure measurement. For the ADC used in this experiment with an 84 root basis, a sonic resolution of 0.023 m/s or a full scale resolution of 6 ppm was achieved. This far exceeds state-of-the-art pressure resolution and is comparable to the resolution of high quality temperature measurements.

The basic device developed here has many potential applications. For example, it has recently been discovered that a single fluid can propagate sound at more than one speed.[2] The technique used for detecting this unexpected phenomenon did not involve a resonance behavior, but rather the traverse time of flight of pressure-pulse generated waves. If the phenomenon of multiple speeds of sound in a fluid is well-founded, there must be observable resonance effects corresponding to those speeds. The theoretical results in Figure 4-6 show that the ST method would be well suited for investigating this phenomenon.

Also, with sensitive enough detection such that no external excitation is needed, a similar device could simply listen to the noise already in a cavity and from that deduce the speed of sound. For a pipeline in which the fluid is energized by the pumping action, one could detect the speed of sound in a passing fluid by simply listening to the fluid. The fluid motion leads to an apparent separation of sonic speed via the Doppler effect and a ST determination of that separation would lead to a direct measurement of the flow velocity. Since fluid density may be related to the sonic speed, the mass flow rate could also be determined. Combining these with pressure and temperature measurements,

---

[2] J. Bosse, G. Jacucci, M. Ronchetti, and W. Schirmacher, "Fast Sound in Two-Component Liquids" Physical Review Letters 57 (December 1986): 3277.

valuable information about flowing streams could be obtained by passive noninvasive processes. Representatives of the petroleum and pipeline industries have already shown a strong interest in this new art. Negotiations are presently underway to cooperate with these industries in further development of the technique.

Measuring critical phenomena of fluids with sonic techniques is difficult when using a frequency tracking method. When the fluid is close to the critical temperature and density, the mixture approaches a chaotic state and the speed of sound approaches zero. As this occurs, the spectrum collapses and bunches all the frequencies closer together while the speed of sound and resonance frequency are dropping rapidly. It is easy to lose the frequency being tracked since it is moving very rapidly. With the ST, all frequencies would be measured for a given basis set of roots and then transformed automatically to the sonic domain providing that resonances can be detected.

Another area with good potential for the utilization of a sonic speed meter is that of reaction kinetics. The sonic speed is highly sensitive to all changes in the structure or composition of a material system and thus could be used to monitor the progress of a chemical or physical transformation. The chemical industry has again expressed interest in this newly evolving technology as a possible

means of remotely following the kinetics of a complex polymerization reaction in large batch reactor.

The applications that have been mentioned thus far are only a few of the possibilities for this new technique. To list all potential possibilities would be like listing all of the applications of a thermometer. The most important result of this study is the application of an ideal numerical model of a physical phenomena to a real experiment. The data of many phenomena can be transferred from an arbitrary domain to a domain that communicates more information. For example, these same principles could relate molecular geometries to vibrational spectra or trajectories to ion cyclotron resonance spectra. Any phenomenon that has an ideal or reference state model could be transformed to an ideal domain. The frequency domain spectra are necessary for investigation of fine structure. In fact, the transform to an ideal domain should demonstrate these deviations readily.

The availability of fast computational processes has facilitated this blend of theory and experiment on a numerical level. Since modern modeling techniques generally involved numerical solutions, it is natural that the communication of these theories to experiments should also be numerical. This experiment is representative of the current influence of numerical mathematics on scientific research, which will significantly change the perceptions

and interpretations of future physical experiments. In the future, numerical mathematics should not be avoided in applications of experimental science, but rather employed vigorously throughout all of experimental science.

APPENDIX A
FAST FOURIER TRANSFORM SOURCE CODE

```
      IMPLICIT REAL*8(A-H,O-Z)
      IMPLICIT INTEGER*4 (I-N)
      INTEGER*2 HEX(256),HIGH,LOW,TAF(16384)
      CHARACTER*1 A(64)
      CHARACTER*20 FILENAME,FILEOUT
      DIMENSION XR(65536),XI(65536)
      COMMON XMAX,PI,NU,NDP,NDPDIV2,NDPDIV4,NDPMIN1,IND
C USE FFT TRANSFORM WITH REAL DATA IN XR ARRAY
      PI=2.0*ACOS(0.0)
      NU=16
      NDP=2**NU
      NREAD=1024
      NDPDIV2=NDP/2
      NDPDIV4=NDP/4
      NDPMIN1=NDP-1
      IND=-1
      CALL HEXGET(HEX)
C START TIME AVG
      DO 20 IF=100,599
      WRITE(FILENAME,'(A8,I3,A4)') 'E:\\HEX\\F',IF,'.OUT'
      OPEN(10,FILE=FILENAME,STATUS='OLD')
      READ(10,*) T,P
      DO 30 I=1,NREAD
         READ(10,300) (A(K),K=1,64)
  300    FORMAT(64A1)
         DO 50 K=2,64,2
            HIGH=HEX(ICHAR(A(K-1)))*16
            LOW=HEX(ICHAR(A(K)))
            XR((I-1)*32+K/2)=FLOAT(HIGH+LOW)
   50    CONTINUE
   30 CONTINUE
      CLOSE(10)
      DO 70 I=1,NDPDIV2
         XR(NDPDIV2+I)=XR(I)
   70 CONTINUE
      CALL BASELINE(XR,XI)
      CALL BLACK(XR)
      CALL FFT(XR,XI)
      XMAX=0.0
      DO 41 L=1,400
         XR(L)=0
   41 CONTINUE
```

```
      DO 40 L=101,NDPDIV2
         XMAX=AMAX1(XMAX,XR(L))
   40 CONTINUE
      DO 60 L=2,NDPDIV2,2
         TAF(L/2)=INT((XR(L)+XR(L-1))/XMAX*8192)
   60 CONTINUE
      WRITE(FILEOUT,'(A7,I3,A4)') 'E:\\FD\\F',IF,'.FFT'
      WRITE(*,200) FILEOUT
      OPEN(10,FILE=FILEOUT,FORM='UNFORMATTED')
      WRITE(10) T,P
      WRITE(10) TAF
      CLOSE(10)
   20 CONTINUE
   200 FORMAT(A)
      END


C*************************************************************
C234567
      SUBROUTINE BASELINE(XR,XI)
      IMPLICIT REAL*8(A-H,O-Z)
      IMPLICIT INTEGER*4 (I-N)
      DIMENSION XR(1),XI(1)
      COMMON XMAX,PI,NU,NDP,NDPDIV2,NDPDIV4,NDPMIN1,IND
      ARX = 0.0
      DO 100 I = 1 , NDP
        ARX = ARX + XR(I)
  100 CONTINUE
      ARX = ARX / FLOAT(NDP)
      DO 200 I = 1,NDP
        XR(I) = XR(I) - ARX
  200 CONTINUE
      DO 300 I=1,NDP
         XI(I)=0.0
  300 CONTINUE
      RETURN
      END

C*************************************************************
      SUBROUTINE BLACK(XR)
      IMPLICIT REAL*8(A-H,O-Z)
      DIMENSION XR(1)
      COMMON XMAX,PI,NU,NDP,NDPDIV2,NDPDIV4,NDPMIN1,IND
      DO 100 I = 1,NDP
        C = 2.0*PI*FLOAT(I)/FLOAT(NDP)
        A = 0.49755 * COS(C)
        B = 0.07922 * COS(2.0*C)
        XR(I) = XR(I) * (0.42423 - A + B)
  100 CONTINUE
      RETURN
      END
```

```
C***********************************************
      SUBROUTINE FFT(XR,XI)
      IMPLICIT REAL*8(A-H,O-Z)
      IMPLICIT INTEGER*4 (I-N)
      DIMENSION XR(1),XI(1)
      COMMON XMAX,PI,NU,NDP,NDPDIV2,NDPDIV4,NDPMIN1,IND
      DO 100 L = 1,NU
           LE = 2**(NU+1-L)
           LE1 = LE/2
           U1 = 1.0
           U2 = 0.0
           ARG = PI/LE1
           C = COS (ARG)
           S = IND*SIN(ARG)
           DO 101 J = 1,LE1
              DO 102 I = J,NDP,LE
                 IP = I + LE1
                 T1 = XR(I) + XR(IP)
                 T2 = XI(I) + XI(IP)
                 T3 = XR(I) - XR(IP)
                 T4 = XI(I) - XI(IP)
                 XR(IP) = T3*U1-T4*U2
                 XI(IP) = T4*U1+T3*U2
                 XR(I) = T1
                 XI(I) = T2
 102          CONTINUE
              U3 = U1*C-U2*S
              U2 = U2*C+U1*S
              U1 = U3
 101       CONTINUE
 100     CONTINUE
         J = 1
         DO 104 I = 1,NDPMIN1
           IF (I .GE. J) GOTO 25
           TEMP = XR(I)
           XR(I) = XR(J)
           XR(J) = TEMP
           TEMP = XI(I)
           XI(I) = XI(J)
           XI(J) = TEMP
 25         K = NDPDIV2
 20         IF (K .GE. J) GOTO 30
           J = J-K
           K = K/2
           GOTO 20
 30        J = J + K
 104     CONTINUE
           DO 60 I = 1 , NDPDIV2
              XR(I) = SQRT(XR(I)*XR(I)+XI(I)*XI(I))
 60        CONTINUE
      RETURN
      END
```

```
C*************************************************************
***
      SUBROUTINE HEXGET(HEX)
      IMPLICIT REAL*8(A-H,O-Z)
      IMPLICIT INTEGER*4 (I-N)
      INTEGER*2 HEX(256)
      HEX(ICHAR(' '))=0
      HEX(ICHAR('0'))=0
      HEX(ICHAR('1'))=1
      HEX(ICHAR('2'))=2
      HEX(ICHAR('3'))=3
      HEX(ICHAR('4'))=4
      HEX(ICHAR('5'))=5
      HEX(ICHAR('6'))=6
      HEX(ICHAR('7'))=7
      HEX(ICHAR('8'))=8
      HEX(ICHAR('9'))=9
      HEX(ICHAR('A'))=10
      HEX(ICHAR('B'))=11
      HEX(ICHAR('C'))=12
      HEX(ICHAR('D'))=13
      HEX(ICHAR('E'))=14
      HEX(ICHAR('F'))=15
      RETURN
      END
```

APPENDIX B
SONIC TRANSFORM SOURCE CODE

```
      IMPLICIT REAL*8 (A-H,O-Z)
      DIMENSION ROOT(84),SMAG(16384),T(500),P(500)
      INTEGER*2 CO(16384),C,SPO(16384)
      CHARACTER*20 FILEIN,FILEOUT
      TWOPI=4.0*ACOS(0.0)
      CALL RTGET(ROOT)
      TAVG=0.0
      PAVG=0.0
      NROOT=84
      CMAX=200.0*TWOPI*3.0*2.54/ROOT(NROOT)
      CRES=CMAX/16384.0
      NMAX=16384
      FRES=20000.0/16384
      DENOM=TWOPI*3.0*2.54/100*FRES
    DO 40 I=100,599
      INDX=I-99
      WRITE(FILEIN,'(A7,I3,A4)') 'E\:\\FD\\F',I,'.FFT'
      WRITE(*,100) FILEIN
100   FORMAT(A)
      OPEN(1,FILE=FILEIN,FORM='UNFORMATTED')
      READ(1) T(INDX),P(INDX)
      READ(1) CO
      CLOSE(1)
      XMAX=0.0
      DO 10 C=1,NMAX
         SPEED=FLOAT(C)*CRES
         RATIO=SPEED/DENOM
         SMAG(C)=0.0
         DO 20 J=1,NROOT
            INDEX=INT(RATIO*ROOT(J)+0.5)
            IF(INDEX.GT.16384) THEN
              TEMP=0.0
            ELSE
              TEMP=DBLE(CO(INDEX))
            ENDIF
            SMAG(C)=SMAG(C)+TEMP
20       CONTINUE
         XMAX=AMAX1(XMAX,SMAG(C))
10    CONTINUE
      DO 30 C=1,NMAX
         SPO(C)=INT(SMAG(C)/XMAX*16384.0)
30    CONTINUE
```

```
      WRITE(FILEOUT,'(A7,I3,A4)') 'E\:\\SD\\F',I,'.SPD'
      OPEN(1,FILE=FILEOUT,FORM='UNFORMATTED')
      WRITE(1) T(INDX),P(INDX)
      WRITE(1) SPO
      CLOSE(1)
      TAVG=TAVG+T(INDX)
      PAVG=PAVG+P(INDX)
      WRITE(*,*) T(INDX),P(INDX)
 40   CONTINUE
      TAVG=TAVG/500.0
      PAVG=PAVG/500.0
      SDT=0.0
      SDP=0.0
      DO 50 I=1,500
         SDT=SDT+(TAVG-T(I))**2
         SDP=SDP+(PAVG-P(I))**2
 50   CONTINUE
      SDT=SDT/499.0/500.0
      SDT=1.96*SQRT(SDT)
      SDP=SDP/499.0/500.0
      SDP=1.96*SQRT(SDP)
      WRITE(*,200) TAVG,SDT,PAVG,SDP
 200  FORMAT(F10.4,'+/-',F7.4,F10.4,'+/-',F7.4)
      WRITE(*,300) CRES
 300  FORMAT('  RESOLUTION OF SONIC DOMAIN=',F10.5)
      END

C
C
C
C
C
C
      SUBROUTINE RTGET(ROOT)
      IMPLICIT REAL*8 (A-H,O-Z)
      DIMENSION ROOT(1)
      ROOT(1)=2.08158
      ROOT(2)=3.34209
      ROOT(3)=4.49341
      ROOT(4)=4.51408
      ROOT(5)=5.64670
      ROOT(6)=5.94036
      ROOT(7)=6.75643
      ROOT(8)=7.28990
      ROOT(9)=7.72523
      ROOT(10)=7.85107
      ROOT(11)=8.58367
      ROOT(12)=8.93489
      ROOT(13)=9.20586
      ROOT(14)=9.84043
      ROOT(15)=10.0102
      ROOT(16)=10.6140
```

```
ROOT(17)=10.9042
ROOT(18)=11.0703
ROOT(19)=11.0791
ROOT(20)=11.9729
ROOT(21)=12.1428
ROOT(22)=12.2794
ROOT(23)=12.4046
ROOT(24)=13.2024
ROOT(25)=13.2956
ROOT(26)=13.4721
ROOT(27)=13.8463
ROOT(28)=14.0663
ROOT(29)=14.2850
ROOT(30)=14.5906
ROOT(31)=14.6513
ROOT(32)=15.2446
ROOT(33)=15.3108
ROOT(34)=15.5793
ROOT(35)=15.8193
ROOT(36)=15.8633
ROOT(37)=16.3604
ROOT(38)=16.6094
ROOT(39)=16.9776
ROOT(40)=17.0431
ROOT(41)=17.1176
ROOT(42)=17.2207
ROOT(43)=17.4079
ROOT(44)=17.9473
ROOT(45)=18.1276
ROOT(46)=18.3565
ROOT(47)=18.4527
ROOT(48)=18.4682
ROOT(49)=18.7428
ROOT(50)=19.2628
ROOT(51)=19.2704
ROOT(52)=19.4964
ROOT(53)=19.5819
ROOT(54)=19.8625
ROOT(55)=20.2219
ROOT(56)=20.3714
ROOT(57)=20.4065
ROOT(58)=20.5379
ROOT(59)=20.5596
ROOT(60)=20.7960
ROOT(61)=21.2312
ROOT(62)=21.5372
ROOT(63)=21.5779
ROOT(64)=21.6667
ROOT(65)=21.8401
ROOT(66)=21.8997
ROOT(67)=22.0000
ROOT(68)=22.5781
```

```
ROOT(69)=22.6165
ROOT(70)=22.6625
ROOT(71)=23.0829
ROOT(72)=23.1067
ROOT(73)=23.1950
ROOT(74)=23.3906
ROOT(75)=23.5194
ROOT(76)=23.6534
ROOT(77)=23.7832
ROOT(78)=23.9069
ROOT(79)=24.3608
ROOT(80)=24.3821
ROOT(81)=24.4749
ROOT(82)=24.6899
ROOT(83)=24.8503
ROOT(84)=24.8995
RETURN
END
```

APPENDIX C
EQUATION OF STATE FOR ARGON
SOURCE CODE

```
      IMPLICIT REAL*8 (A-H,O-Z)
      REAL*8 B(100),B1(100),B2(100),T(100)
      REAL*8 C(100),C1(100),C2(100),BD(100),N
      EPK=119.8D 00
      B0=49.80D-03
      PCON=6.8046D-02
      KEL=273.15
      OPEN (10,FILE='E\:\\SOURCE\\TVC.CON',STATUS='OLD')
      DO 25 I=1,74
      READ(10,*)
     CT(I),B(I),B1(I),B2(I),BD(I),C(I),C1(I),C2(I)
 25   CONTINUE
      CLOSE (10)
 100  WRITE(*,*) ' INPUT TEMPERATURE (Celcius) AND
     CPRESSURE (psia)'
      READ(*,*) TEMP,P
      P=P*PCON
      TEMP=TEMP+KEL
      TS=TEMP/EPK
      CALL
     CQAND(BS,BS1,BS2,BSD,CS,CS1,CS2,TS,T,
     CB,B1,B2,BD,C,C1,C2)
      BV=BS*B0
      CV=CS*B0*B0
      CALL VERVOL(P,V,TEMP,BV,CV)
      VS=V/B0
      CALL SPEED(CAR,TEMP,BS,BS1,BS2,BSD,CS,CS1,CS2,VS)
      WRITE(*,*) ' SPEED=',CAR
      GOTO 100
      END
C
C
C
C
C
C
C
      SUBROUTINE
     CQAND(BS,BS1,BS2,BSD,CS,CS1,CS2,TS,T,B,B1,B2
     C,BD,C,C1,C2)
      IMPLICIT REAL*8 (A-H,O-Z)
```

```
      REAL*8 B(1),B1(1),B2(1),T(1),C(1),C1(1),C2(1),BD(1)
      REAL*8 M
      DO 20 I=2,74
       IF (TS.GT.T(I-1).AND.TS.LT.T(I)) THEN
        M=(TS-T(I-1))/(T(I)-T(I-1))
        BS=B(I-1)+M*(B(I)-B(I-1))
        BS1=B1(I-1)+M*(B1(I)-B1(I-1))
        BS2=B2(I-1)+M*(B2(I)-B2(I-1))
        BSD=BD(I-1)+M*(BD(I)-BD(I-1))
        CS=C(I-1)+M*(C(I)-C(I-1))
        CS1=C1(I-1)+M*(C1(I)-C1(I-1))
        CS2=C2(I-1)+M*(C2(I)-C2(I-1))
        RETURN
       ENDIF
 20    CONTINUE
      WRITE(*,*)'TSTAR OUT OF RANGE'
      RETURN
      END
C
C
C
C
C
C
C
      SUBROUTINE VERVOL(P,V,T,B,CV)
      IMPLICIT REAL*8 (A-H,O-Z)
      R=8.20575D-02
      TOL=1.0D-16
C INPUT P IN ATM
C INPUT T IN KELVIN
      V=R*T/P
 10   VN=R*T/P*(1.0D 00 + B/V + CV/V/V)
      TEST=V/VN
      IF(TEST.GT.1.0) THEN
      TEST=1.0D 00 - 1.0D 00/TEST
      ELSE
      TEST=1.0D 00 -TEST
      ENDIF
      V=VN
      IF(TEST.GT.TOL)  GOTO 10
      RETURN
      END
C
C
C
C
C
C
C
      SUBROUTINE SPEED(C,T,BS,BS1,BS2,BSD,CS,CS1,CS2,VS)
      IMPLICIT REAL*8 (A-H,O-Z)
```

```
      REAL*8 M,DSQRT
      M=39.948D-03
      R=8.31441D 00
      GAMA=
     C5.0D0/2.0D0-BS2/VS+(BSD*BSD-CS+CS1-0.5D0*CS2)/VS/VS
      GAMA=GAMA/(3.0D0/2.0D0-(2.0D0*BS1+BS2)/VS-
    @(2.0D0*CS1+CS2)/2.0D0/VS/VS)
      C=GAMA*R*T/M*(1.0D 00+2.0D0*BS/VS+3.0D0*CS/VS/VS)
      C=DSQRT(C)
      RETURN
      END
```

APPENDIX D
DATA ACQUISITION SOURCE CODE

```
#include <stdio.h>
#include <stdlib.h>
#include <math.h>
#include <string.h>
#include "DECL.H"                /* supplied with driver
libraries */
#include <time.h>
#include <sys/timeb.h>
#include <sys/types.h>
#include <conio.h>

#define    PORT0    0x178        /* default setting      */
#define    PORT1    0x179        /* all switches are off */
#define    PORT2    0x17A
#define    PORT3    0x17B
#define    COMMA    0x2c
#define    NOERR    0

/*****************************/
/* driver library functions */
/*****************************/
extern int ibfind();
extern void ibtmo();
extern void ibclr();
extern void ibeos();
extern void ibrd();
extern void ibwrt();
extern void ibcmd();
extern void ibsic();
extern void ibloc();
extern void ibrsp();
extern void ibwait();

FILE *stream;
char *dacoutput=(char*)0xD0000000;
int addr=0x20;

unsigned char io[32768];
long timeout[500];
float pout[500];
double tout[500];
long t,t0,tday;
```

```
/*******************************************/
/* sends temperature in celcius to the oven, */
/*******************************************/
void wrtoven(float setpoint)
{
int j,ovn;
char ostring[14],fp[10];
    gcvt(setpoint,5,fp);
    strcpy(ostring,"setpoint ");
    ostring[9]=fp[0];
    ostring[10]=fp[1];
    ostring[11]=fp[2];
    ostring[12]=fp[3];
    ostring[13]=fp[4];
    ostring[14]='\0';
    ovn = ibfind("oven");
    ibwrt( ovn, ostring, 15);
    printf(" %s\n",ostring);
    return;
}


/*******************************************/
/* reads temp in celcius form rtd,          */
/*******************************************/
double rdrtd()
{
int i,rtd;
double res,rc,aldel,pt1,pt2,pt3,pt4,t2;
double r0=99.98;
double alpha=0.0039076;
double delta=1.5205;
char rstring[16];
    rtd = ibfind("k195a");
    ibrd( rtd, rstring, 17 );
    for(i=0; i<4; i++) rstring[i]=' ';
    for(i=15; i<17; i++) rstring[i]=' ';
    res=atof(rstring);
    aldel=alpha*delta;
    rc=res/r0;
    rc=rc-1.0;
    pt1=aldel/100.0;
    pt1=pt1+alpha;
    pt2=pt1*pt1;
    pt3=4.0*rc;
    pt3=pt3*aldel;
    pt3=pt3/10000.0;
    pt4=2.0*aldel;
    pt4=pt4/10000.0;
    t2=sqrt(pt2-pt3);
    t2=pt1-t2;
```

```
    return (t2/pt4);
}


/*******************************************/
/*     reads the pressure transducer,      */
/*******************************************/

float rdpress()
{
int ptrans;
  char pstring[9];
  ptrans = ibfind("beckman");
  ibrd( ptrans, pstring, 10 );
  pstring[7]=' ';
  pstring[8]=' ';
  pstring[9]=' ';
  return (atof(pstring));
}

/*********************************/
/* gets the time in milliseconds  */
/*********************************/

void get_milli()
{
  char tmp[1];
  long h,m,s;

  struct timeb timebuffer;
  char *timeline;

  ftime(&timebuffer);
  timeline = ctime(&(timebuffer.time));

  tmp[0]=timeline[11];
  tmp[1]=timeline[12];
  h=atol(tmp);
  h=h*3600;
  tmp[0]=timeline[14];
  tmp[1]=timeline[15];
  m=atol(tmp);
  m=m*60;
  tmp[0]=timeline[17];
  tmp[1]=timeline[18];
  s=atol(tmp);
  t=h+m;
  t=t+s;
  t=t*1000;
  t=t+timebuffer.millitm;
  s=t-t0;
  if(s < 0 ) {
```

```
    t0=t0-tday;
    t=t-t0;}
  else t=s;
  return;

}

/************************************/
/*   collects data from dac         */
/*                                  */
/************************************/

unsigned int  sample(size)
    unsigned int size;
 {
    int busy;
    int count;

    outpw(PORT2,0xa03f);        /* initialize single input*/
    outpw(PORT0,0xffff);        /* clear counter */
    outpw(PORT0,0xffff);
    count = -(size + 0xff);     /* correct count */
    outpw(PORT0,count);         /* load count */
    outpw(PORT0,count);
    outp(PORT2, 0x3c);          /* start the counter
20kHz,40kHz*/

    busy = inp(PORT2);          /* wait for sampling to be
completed */
    while (busy == inp(PORT2));/* sampling is done */

    outp(PORT2,0x3f);           /* enabled WAAGII ram */
    return(inpw(PORT0));        /* read trigger address */
  }

/************************************************/
/* clears HP-IB, initializes instrument timeout */
/* initializes varibles                         */
/************************************************/
void init()
{
    tday=0;
    t0=0;
    get_milli();
    tday=24*3600;
    tday=tday*1000;
    t0=t;
    return;
}


main()
```

```
{
char filename[8],num[2];
unsigned int size=16384; /* number of sample points */
unsigned int trigger,i,j;
unsigned short ih,il,ihigh,index,iloop,nloop;
float setpoint,step;

unsigned int sample(unsigned int);
void wrtoven(float);
double rdrtd(void);
float rdpress(void);
void get_milli(void);
void init(void);

  init();
/*  step=0.01;*/
  step=0.0;
  printf(" input setpoint -0.09 > # > 0.09\n");
  scanf("%f",&setpoint);
  nloop=600;
  for(iloop=100; iloop<nloop; iloop++) {
    index=iloop-100;

    tout[index]=rdrtd();
    printf("%.3f celcius ",tout[index]);

    pout[index]=rdpress();
    printf(" %.1f PSI ",pout[index]);

    trigger = sample(size);   /* data acquisition */
    for(i=0; i<size*2; i++) io[i] = *(dacoutput+i);
    gcvt(iloop,3,num);
    filename[0]='f';
    filename[1]=num[0];
    filename[2]=num[1];
    filename[3]=num[2];
    filename[4]='.';
    filename[5]='d';
    filename[6]='a';
    filename[7]='t';
    filename[8]='\0';
    printf(" filename= %s ",filename);
    stream=fopen(filename,"ab");
    fwrite((char *)io,sizeof(unsigned char),32768,stream);
    fclose(stream);

    get_milli();
    timeout[index]=t;
    printf(" %ld msec ",timeout[index]);

    setpoint=setpoint-step;
    wrtoven(setpoint);
```

```
 }
 stream = fopen("temp.out", "wb");
 fwrite((char *)tout,sizeof(double),500,stream);
 fclose(stream);

 stream = fopen("press.out", "wb");
 fwrite((char *)pout,sizeof(float),500,stream);
 fclose(stream);

 stream = fopen("time.out", "wb");
 fwrite((char *)timeout,sizeof(long),500,stream);
 fclose(stream);
}
```

APPENDIX E
DATA CONVERSION SOURCE CODE

```
#include <stdio.h>
#include <string.h>
#include <stdlib.h>

FILE *stream;

unsigned char io[32768];
double tout[500];
float pout[500];
char filein[15],fileout[15];


main()

{
unsigned int index,i,j,k;
char num[2];

 stream = fopen("e:\\raw\\temp.out", "rb");
 fread((char *)tout,sizeof(double),500,stream);
 fclose(stream);

 stream = fopen("e:\\raw\\press.out", "rb");
 fread((char *)pout,sizeof(float),500,stream);
 fclose(stream);

  for(i=100; i<600; i++) {
    index=i-100;

    gcvt(i,3,num);
    filein[0]='e';
    filein[1]='\:';
    filein[2]='\\';
    filein[3]='r';
    filein[4]='a';
    filein[5]='w';
    filein[6]='\\';
    filein[7]='f';
    filein[8]=num[0];
    filein[9]=num[1];
```

```
    filein[10]=num[2];
    filein[11]='.';
    filein[12]='d';
    filein[13]='a';
    filein[14]='t';
    filein[15]='\0';

    stream=fopen(filein,"rb");
    fread((char *)io,sizeof(unsigned char),32768,stream);
    fclose(stream);

    fileout[0]='e';
    fileout[1]='\:';
    fileout[2]='\\';
    fileout[3]='h';
    fileout[4]='e';
    fileout[5]='x';
    fileout[6]='\\';
    fileout[7]='f';
    fileout[8]=num[0];
    fileout[9]=num[1];
    fileout[10]=num[2];
    fileout[11]='.';
    fileout[12]='o';
    fileout[13]='u';
    fileout[14]='t';
    fileout[15]='\0';

    stream=fopen(fileout,"w");
    fprintf(stream,"%.3f %.1f",tout[index],pout[index]);
    printf("%u %.3f %.1f\n",index,tout[index],pout[index]);

    for(j=0; j<1024; j++){
      fprintf(stream,"\n");
      for(k=0; k<32; k++) fprintf(stream,"%2X",io[j*32+k]);
    }
    fclose(stream);
  }
}
```

BIBLIOGRAPHY

Bergland, G.D. "A Fast Fourier Transform Algorithm for Real-Valued Series." Communications of the ACM 11 (October 1968): 703-710.

Bird, R. Byron. "Numerical Evaluation of the Second Virial Coefficient." The Virial Equation of State CM-599. Madison: University of Wisconsin, May 10, 1950.

Bosse, J., Jacucci, G., Ronchetti, M., and W. Schirmacher. "Fast Sound in Two-Component Liquids." Physical Review Letters 57 (December 1986): 3277-3279.

Colclough, A.R. "Systematic Errors in Primary Acoustic Thermometry in the Range 2-20 K." Metrologia 9 (1973): 75-98.

Colgate, S.O., Sona, C.F., Reed, K.R., and A. Sivaraman. "Experimental Ideal Gas Reference State Heat Capacities of Gases and Vapors." Journal of Chemical and Engineering Data 35 (1990): 1-5.

Colgate, S.O., Williams, K.R., Reed, K., and C. Hart. "C_p/C_v Ratios by the Sound Velocity Method Using a Spherical Resonator." Journal of Chemical Education 64 (June 1987): 553-556.

Cooley, J.W., and J.W. Tukey. "An Algorithm for the Machine Calculation of Complex Fourier Series." Mathematical Computations 19 (April 1965): 297-301.

Ewing, M.B., Goodwin, A.R.H., and J.P.M. Trusler. "Thermophysical Properties of Alkanes from Speeds of Sound Determined Using a Spherical Resonator 3. n-pentane." Journal of Chemical Thermodynamics 21 (1989): 867-877.

Ewing, M.B., McGlashan, M.L., and J.P.M. Trusler. "The Temperature-Jump Effect and the Theory of the Thermal Boundary Layer for a Spherical Resonator, Speeds of Sound in Argon at 273.16 K." Metrologia 22 (1986): 93-102.

Ferris, H.G. "The Free Vibrations of a Gas Contained within a Spherical Vessel." Journal of the Acoustical Society of America 24 (January 1952): 57-65.

Golub, G.H., and C.F. Van Loan. Matrix Computations. Baltimore: Johns Hopkins University Press, 1985.

Hirschfelder, J.O., Curtiss, C.F., and R.B. Bird. Molecular Theory of Gases and Liquids. New York: Wiley and Sons, 1954.

Mehl, J.B., and M.R. Moldover. "Precision Acoustic Measurements with a Spherical Resonator: Ar and C_2H_4." Journal of Chemical Physics 74 (April 1981): 4062-4077.

Mehl, J.B., and M.R. Moldover. "Precondensation Phenomena in Acoustic Measurements." Journal of Chemical Physics 77 (July 1982): 455-465.

Moldover, M.R., Mehl, J.B., and M. Greenspan. "Gas-Filled Spherical Resonators: Theory and Experiment." Journal of the Acoustical Society of America 79 (February 1986): 253-271.

Rayleigh, J.W.S. Theory of Sound. New York: Dover, 1894, reprinted 1945.

Tewfik, A.H., Levy, B.C., and A.S. Willsky. "An Eigenstructure Approach for the Retrieval of Cylindrical Harmonics." Signal Processing 13 (September 1987): 121-139.

BIOGRAPHICAL SKETCH

Kenneth C. McGill was born June 6, 1957, in Port Arthur, Texas, the youngest child and second son of Martha and Edward McGill. Ken moved to Topeka, Kansas, at the age of three where he attended grade school, junior and senior high. Upon graduation from Topeka West High and Kaw Valley Area VoTech in 1975, Ken worked as a weldor for several factories in the Topeka area. In 1979, Ken returned to school, attending Washburn University in Topeka while also serving as a reservist in the Air National Guard. He graduated magna cum laude (G.P.A. of 3.67 of 4.00) in 1985 with dual B.S. degrees in physics and chemistry.

In 1985, Ken entered the University of Florida as a doctoral student in physical chemistry. He studied quantum theory for about two years under Yngve Ohrn before joining Dr. S.O. Colgate's experimentalist group. Principal areas of research interest are currently data acquisition techniques in acoustic measurements, thermodynamics of acoustics and fluid mixtures. Upon graduation, Ken has earned a one-year post-doctoral position with Dr. Colgate to further investigate Sonic Transformation techniques.

Ken, a widower, has recently remarried and he and his wife are expecting their first child in March 1991.

I certify that I have read this study and that in my opinion it conforms to acceptable standards of scholarly presentation and is fully adequate, in scope and quality, as a dissertation for the degree of Doctor of Philosophy.

Samuel O. Colgate, Chairman
Associate Professor of Chemistry

I certify that I have read this study and that in my opinion it conforms to acceptable standards of scholarly presentation and is fully adequate, in scope and quality, as a dissertation for the degree of Doctor of Philosophy.

N. Yngve Ohrn, Cochairman
Professor in Chemistry and Physics

I certify that I have read this study and that in my opinion it conforms to acceptable standards of scholarly presentation and is fully adequate, in scope and quality, as a dissertation for the degree of Doctor of Philosophy.

Thomas Bailey
Professor of Physics

I certify that I have read this study and that in my opinion it conforms to acceptable standards of scholarly presentation and is fully adequate, in scope and quality, as a dissertation for the degree of Doctor of Philosophy.

John R. Eyler
Professor of Chemistry

I certify that I have read this study and that in my opinion it conforms to acceptable standards of scholarly presentation and is fully adequate, in scope and quality, as a dissertation for the degree of Doctor of Philosophy.

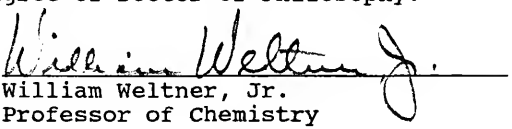

William Weltner, Jr.
Professor of Chemistry

This dissertation was submitted to the Graduate Faculty of the Department of Chemistry in the College of Liberal Arts and Sciences and to the Graduate School and was accepted as partial fulfillment of the requirements for the degree of Doctor of Philosophy.

December 1990

Dean, Graduate School

UNIVERSITY OF FLORIDA
3 1262 08553 4484